GRAVITATIONAL WAVES AS A NOVEL PROBE IN SEARCH OF NEW PHYSICS

A THESIS

submitted in partial fulfillment of the requirements

for the award of the dual degree of

Bachelor of Science-Master of Science

in

PHYSICS

by

RAI RIYA AJAYKUMAR

(19234)

DEPARTMENT OF PHYSICS
INDIAN INSTITUTE OF SCIENCE EDUCATION AND RESEARCH
BHOPAL
BHOPAL - 462066

April 2024

भारतीय विज्ञान शिक्षा एवं अनुसंधान संस्थान भोपाल
Indian Institute of Science Education and Research
Bhopal
(Estb. By MHRD, Govt. of India)

CERTIFICATE

This is to certify that **Rai Riya Ajaykumar**, BS-MS (Dual Degree) student in Department of Physics, has completed bonafide work on the thesis entitled **'Gravitational Waves as a Novel Probe in Search of New Physics'** under my supervision and guidance. The content of this report is original and has not been submitted elsewhere for the award of any academic or professional degree.

April 2024
IISER Bhopal

Dr. Rahul Srivastava

Committee Member	Signature	Date

ACADEMIC INTEGRITY AND COPYRIGHT DISCLAIMER

I hereby declare that this project is my own work and, to the best of my knowledge, it contains no materials previously published or written by another person, or substantial proportions of material which have been accepted for the award of any other degree or diploma at IISER Bhopal or any other educational institution, except where due acknowledgement is made in the document.

I certify that all copyrighted material incorporated into this document is in compliance with the Indian Copyright (Amendment) Act (2012) and that I have received written permission from the copyright owners for my use of their work, which is beyond the scope of the law. I agree to indemnify and save harmless IISER Bhopal from any and all claims that may be asserted or that may arise from any copyright violation.

April 2024 **Rai Riya Ajaykumar**

IISER Bhopal

ACKNOWLEDGEMENTS

I wish to thank my thesis supervisor Dr. Rahul Srivastava, Dept. of Physics, IISER Bhopal for his constant guidance throughout the project and believing that I had the ability to work on this topic. It was his vision backed by expertise and experience in particle phenomenology, that played a pivotal role in shaping this thesis. I have learnt a lot from his perspective towards understanding physics and it will stay with me forever.

I would like to express my deep gratitude towards my institution, Indian Institute of Science Education and Research Bhopal for providing me the infrastructure, research exposure and facilities that made a conducive environment for me to conduct research.

I consider myself fortunate to have friendly and supportive senior members in the research group- Anirban, Hemant, Praveen, Ranjeet and Sushant. I would like to thank all of them for helping and mentoring me from time to time, making this learning curve a lot easier. I would like to thank Debalina, a former menber of the research group for introductory discussions on the project.

I wish to thank my dearest friends- Vedant, Deependra and Sukriti who always had my back during academic and emotional challenges. I feel blessed to have their company.

Finally, I want to thank Aai and Baba for nurturing the love for science in me right from childhood, motivating me to pursue research and supporting me throughout, which has made me worthy enough to work on this thesis.

Rai Riya Ajaykumar

ABSTRACT

In this thesis, we present gravitational waves (GWs) as a new observational signature of the first order cosmological phase transitions that might have occurred in the early universe, thus looking further beyond the energy scales achieved by particle colliders today. Using the python package `CosmoTransitions`, we compute the phase transition parameters like nucleation rate and latent heat fraction in order to plot the GW spectra. We study the gravitational wave spectra produced by individual scalar, fermion and vector boson particle extensions of the standard model to observe that the SM + Scalar and SM + Scalar + Vector Boson case produce GWs detectable by upcoming detectors like LISA, DECIGO and BBO. Furthermore, we consider physically constrained scalar and fermionic DM cases to observe that while the former produces observable GWs, the latter models do not have strong enough first order phase transitions to produce the same, even under a U(1) gauge boson extension. However for the case of SM + Scalar + Scalar DM model, no phase transition is found. Our study hence validates that observing such GWs can not only establish the presence of BSM physics but also probe into the exact nature of the new particle(s) and subsequently inform us of the complete theory of the universe.

LIST OF SYMBOLS AND ABBREVIATIONS

α_{GW}	Latent heat fraction of the phase transitions
β	Nucleation Rate
κ_{SW}	Latent heat fraction of sound waves
κ_{MHD}	Latent heat fraction of magnetohydrodynamic turbulence.
T_c	Critical Temperature
T_{nuc}	Nucleation Temperature
GW	Gravitational Waves
PT	Phase Transition
FOPT	First Order Phase Transition
SM	Standard Model
BSM	Beyond Standard Model
EWPT	Electroweak Phase Transition
CMB	Cosmic Microwave Background
1PI	1 Particle Irreducible
SW	Sound Waves
MHD	Magnetohydrodynamic
VEV	Vacuum Expectation Value
SSB	Spontaneous Symmetry Breaking
GWS	Glashow-Weinberg-Salam

LIST OF FIGURES

LIST OF TABLES

CONTENTS

1. INTRODUCTION

The Standard Model (SM) of elementary particles stands as the most successful theory in the history of particle physics. So far, it has effectively explained many observed processes driven by weak, electromagnetic and strong interactions, survived high-precision tests like the electron magnetic dipole moment calculation and is believed to be theoretically self-consistent as well. In spite of its tremendous success, the Standard Model cannot explain phenomena like neutrino oscillations, baryon asymmetry, origin of dark matter etc., and hence falls short of being the complete theory of particle interactions. The quest for finding this complete theory of the universe is ongoing for over a century now. Particle colliders are being used to to probe new high energy BSM particles, but no conclusive evidence for such is found yet. While traditional collider based searches remain valuable, they have limitations in terms of energy scales that can be explored with the current technological advancements. There are other field specific experiments like those in search of neutrinoless double beta decay, dark matter searches, non standard neutrino interactions e.t.c., but none have found any BSM physics till date. It has perhaps become imperative now to explore alternative avenues for probing BSM physics.

Cosmological searches hold great promise in searching for BSM interactions as they can strongly reduce possible cases of BSM models and can precisely determine candidate model parameters [33]. The upcoming gravitational wave detectors like LISA (Laser Interferometer Space Antenna) [17, 10], DECIGO [32, 31] and BBO [16] can prove to be such a new probe for BSM physics. As the universe cools down, temperature dependent terms in the effective potential of the fields cause changes in the structure of the potential. This may lead to shifts in the potential minima (vacuum) of the universe, through energetic phase transitions. Certain phase transitions (first order phase transitions) occur through the formation of bubbles of true vacuum which collide and merge leading to a stochastic gravitational wave background. These primordial GWs are specific to the underlying theory of elementary particles as the effective potential because of which the phase transitions occur, directly depends on the underlying fields. In our universe, we are sure to have undergone atleast one phase transition during electroweak symmetry breaking. Even though the theory of baryogenesis hints towards this transition being

a FOPT, we are still in search of an experimental evidence supporting this hypothesis. Interestingly, SM predicts it to be a smooth or crossover transition, which rules out the possibility of the formation of GWs. However, different extensions to the SM can cause significant changes in the type of phase transitions (PT) and many give rise to FOPTs, thus forming GWs. Hence, various BSM theories can be put to an experimental test if they give rise to GWs with frequencies detectable by the upcoming GW detectors. Thus stochastic primordial gravitational waves can act as a signature for new physics [37].

In this thesis, we study the gravitational wave signals that arise from phase transitions for extensions of the standard model. In chapter 2, we briefly discuss the essential aspects of cosmology, standard electroweak theory and introduce cosmological phase transitions. Subsequently, chapter 3 gives an overview of the theory of gravitational waves and the various sources responsible for the generation of GWs arising from cosmological PTs. In chapter 4, we give a brief discussion for the scalar, fermion and vector + scalar extension by comparing these spectra with the expected sensitivity frequency space of LISA, DECIGO and BBO. Based on the preliminary results, in chapter 5, we then extend our analysis to certain physically relevant BSM cases with the help of the framework discussed in this thesis.

2. COSMOLOGICAL PHASE TRANSITIONS

2.1 Introduction

Cosmological phase transitions are central to modern cosmological studies. They describe phase transitions that may have occurred in the early universe close to the energy scale of the Grand Unified Theory (GUT). Even though these transitions are expected to have occurred during the cosmological era when the universe was opaque, studies suggest that we still might observe imprints of certain transitions in the universe today. Hence the study of cosmological phase transitions has recently gained interest. While cosmology primarily describes two types of phase transitions: (1) Electroweak Phase Transition and (2) QCD Phase Transition, we will only focus our study on the electroweak phase transitions in this thesis. Understanding the subject of electroweak phase transitions and its observable imprints in today's universe demands an in depth knowledge of topics in gravity, cosmology and particle theory.

This section is aimed at making the reader equipped with the fundamentals of cosmological phase transitions in the context of cosmology as well as the Standard Model of particle physics, while gravity is discussed in the next Chapter 3. This chapter begins with a brief description of the modern cosmological universe and is followed by the discussions on the Standard electroweak theory. The chapter then moves forward by discussing how field potentials calculated using the Standard Electroweak Theory can shed light upon the nature of electroweak phase transitions in a universe described by the Standard Model.

2.2 Cosmology

The subject of cosmology was developed to understand the universe we live in, it's origin, dynamics and it's fate described using the fundamental forces of nature. This overview is an excerpt from M. Breitbach's thesis [7] much of which has been inspired from Baumann's lecture notes [5] and Kolb and Turner's standard reference [34] on cosmology.

2.2.1 Spacetime of the Universe

The geometry of the 4-d space time in our universe is described as time ordered slices of 3-d space. In spite of the anisotropies and the clumpy distribution of galaxies seen on small scales, the large scale structure is homogeneous and isotropic to a good approximation. It is this large scale simplicity that enables one to describe these time ordered slices as the those having constant curvature and density throughout space, i.e., being maximally symmetric. One begins by describing the spacetime metric $g_{\mu\nu}$, which for a flat Minkowski space is given by

$$g_{\mu\nu} = \eta_{\mu\nu} \equiv diag(1, -1, -1, -1). \tag{2.1}$$

Using the spacetime 4-vector $dx^\mu = (dt, d\vec{x})$, the invariant distance which is the same for all non-accelerating observers is,

$$ds^2 \equiv g_{\mu\nu} dx^\mu dx^\nu = dt^2 - d\vec{l}^2, \tag{2.2}$$

where is $d\vec{l}^2$ is generally not equal to $d\vec{x}^2$, except in case of a flat spacetime. This brings us to the concept of defining the curvature of space. For a maximally symmetric space, as is the case for our universe, we assign a constant curvature which can be either positive, zero (flat space) or negative as shown in the Figure 2.1. This is better understood mathematically by writing the Friedmann–Lemaître–Robertson–Walker (FLRW) metric as,

$$dl^2 = a(t)^2 \gamma_{ij} dx^i dx^j \tag{2.3}$$

with,

$$\gamma_{ij} = \delta_{ij} + k\frac{x_i x_j}{1 - k|\vec{x}|^2}, k = \begin{cases} 0, & \text{flat} \\ +1, & \text{positive curvature} \\ -1, & \text{negative curvature} \end{cases} \tag{2.4}$$

and a(t) is the scale factor which is time dependent for our 4-d space time, such the strength of the curvature of spacetime is $\frac{1}{a(t)}$. In this study, a motivation to understand this metric and the dynamics of the spacetime (our universe) described by this metric comes from the fact that perturbations in this FLRW metric can be physically perceived as gravitational waves.

Physical and dimensionless (co-moving) co-ordinates are hence related using this scale factor a(t) as $\vec{x}_{phys} = a(t)\vec{x}$. Hence one writes the modified physical velocity as,

$$\dot{\vec{x}}_{phys} = a(t)\dot{\vec{x}} + H\vec{x}_{phys}, \tag{2.5}$$

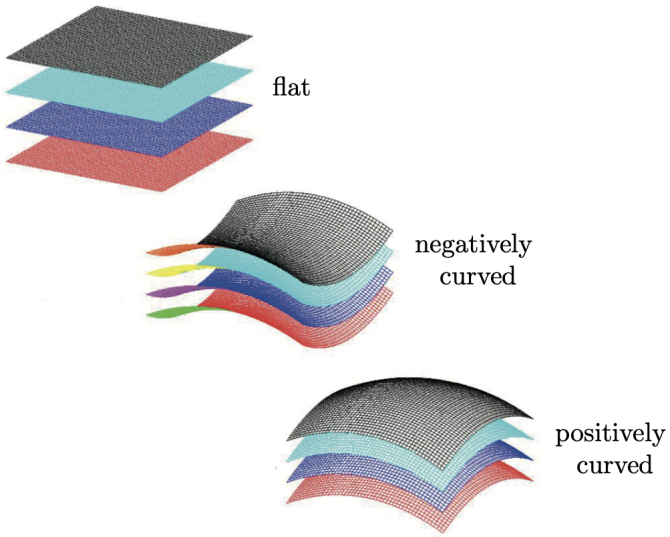

Fig. 2.1: The space-time of our universe can be foliated into flat, negatively curved or positively curved hypersurfaces.

where the time-dependent Hubble parameter is given as,

$$H = \frac{\dot{a}}{a}. \tag{2.6}$$

Positive H contributes to additional velocity proportional to the physical distance of the object and hence describes an expanding universe.

2.2.2 Dynamics of the Spacetime

The General Theory of Relativity gives a framework to describe the local spacetime curvature of based on its energy content. This idea is mathematically expressed in Einstein's field equations,

$$G_{\mu\nu} = 8\pi G T_{\mu\nu}, \tag{2.7}$$

where the local curvature is expressed through Einstein tensor $G_{\mu\nu}$ which is a function of the metric $g_{\mu\nu}$ and its derivatives. The energy content is described by the energy-momentum tensor $T_{\mu\nu}$. These two physical quantities are related through the gravitational constant G$\approx 6.7 \times 10^{-11} m^3 kg^{-1} s^{-2}$ which gives the strength of gravity.
In the FLRW metric, matter is assumed to be a perfect fluid with,

$$T_{\mu\nu} = (\rho + P)\dot{x}_\mu \dot{x}_\nu - P g_{\mu\nu}, \tag{2.8}$$

where ρ is the energy density and P is the fluid pressure. The energy momentum tensor $T_{\mu\nu}$ obeys the continuity equation, which in a curved spacetime is given as,

$$\nabla_\mu T^{\mu\nu} = 0. \tag{2.9}$$

In the FLRW metric, the continuity equation then takes the form,

$$\dot{\rho} + 3H(\rho + P) = 0, \tag{2.10}$$

and talks about the behaviour of energy in expanding space. To understand the dynamics of the universe itself, one uses the field equations 2.7 and inserts the $G_{\mu\nu}$ and $T_{\mu\nu}$ (for a perfect fluid) for the FLRW metric. We hence get the Friedmann equations,

$$H = \frac{\dot{a}}{a} = \sqrt{\frac{8\pi G}{3\rho} - \frac{k}{a^2}}, \tag{2.11}$$

$$\frac{\ddot{a}}{a} = -\frac{4\pi G}{3}(\rho + 3P). \tag{2.12}$$

These equations give a direct relation between the rate of expansion/contraction of the universe and its energy density, fluid pressure and the spacetime curvature. Here ρ is the total energy density which is a sum of ρ_r (radiation), ρ_m (matter both baryonic and cold dark matter) and ρ_Λ (vacuum/dark energy). Using these Friedmann equations, observationally known H_0 value and the flatness our universe, one can now estimate today's distribution of radiation, dark energy (Λ), matter and cold dark matter (CDM) in the universe using the ΛCDM model.

2.2.3 A brief history of the Universe

In this section, I present an overview of the cosmological history of the Universe. The motivation behind mentioning this in the thesis is to appreciate how primordial GWs can help us look deep into the history of the universe. We describe these epochs chronologically starting from moments just after the Big bang, as the universe started cooling down.

1. **Inflationary Epoch:** (t $\approx 10^{-34}$s) Cosmic inflation refers to the accelerated expansion of the universe right after the Big Bang singularity. This idea was developed as a solution to the 'Horizon problem' which discusses the extreme fine-tuning done in all causally connected spaces such that all of them had the same initial temperature. This theory also explains why the universe is largely homogeneous and isotropic. Inflation is described to have started off with a scalar *'inflaton'* field with a specific

potential that induced this inflationary epoch. This *'inflaton'* field then decayed to form other particles, through the process of reheating, after the end of inflation.

2. **Electroweak Phase Transition:** (t ≈ 10ps, T≈ 100 GeV) The physics involved in this era describes how fermions and gauge bosons became massive and is central to the theory of particle physics. The era started off with Spontaneous Symmetry Breaking 2.3.1 as the Higgs field underwent an electroweak phase transition and acquired a new potential minima (vacuum expectation value). In this thesis, we majorly focus on studying the type of phase transition that occurred in this era with the help of the stochastic gravitational radiation that might have been produced during it. If produced, this radiation can help us look at earliest observed timescale of the universe till date.

3. **Baryogenesis:** This period describes a physical process that has been hypothesised to have created matter anti-matter asymmetry. It is said to have taken place during the electroweak phase transition. The theory of baryogenesis is however based on three Sakharov conditions that should be true to create the matter-anti matter asymmetry that we see today. Another requirement for baryogenesis is that the electroweak phase transition should be first order to conserve baryon asymmetry. Our efforts towards finding detectable GWs from FOPT thus serves another purpose of observationally verifying one of the key conditions required for baryogenesis.

4. **QCD Phase Transition:** (t ≈ 10 μs , T≈ 150 MeV) This era highlights the period when the deconfined quarks and gluons went through a phase transition that formed the quark gluon plasma. Subsequently, they confined to form hadrons.

5. **Neutrino Decoupling:**(t ≈ 1s , T≈ 1MeV) Neutrinos which were initially coupled to the thermal bath leave while still being relativistic.

6. **Electron-positron Annihilation:** (t ≈ 6s, T≈ 500 keV) Electrons and positrons annihilated and the energy was absorbed by photons.

7. **Big Bang Nucleosynthesis:** (t ≈ 3min, T≈ 100 keV) Light elements were synthesized during this era.

8. **Recombination and Photon Decoupling:** (t ≈ 380kyr, T≈ 0.28 eV) During this period, hydrogen was formed as electrons and protons recombined and formed photons as a byproduct. These photons were finally able to travel through the whole universe, which we now call the Cosmic Microwave Background (CMB) radiation. Looking further back beyond this point may now be possible by detecting primordial gravitational waves.

2.3 Standard Electroweak (GWS) Theory

During 1967-68, Weinberg and Salam independently formulated the unified theory of electromagnetic and weak interactions, together known as the Electroweak Theory. During that time, even though the idea behind using gauge fields for describing particles was quite popular, little was known about how these fields can be made massive. This was because adding any mass term for gauge bosons in the electroweak interactions would not leave the Lagrangian gauge-invariant.

Hence, the Glashow-Weinberg-Salam Model was formulated to generate mass for the gauge bosons through Spontaneous Symmetry Breaking (SSB), while also ensuring that the theory is renormalizable. Specifically, the $SU(2)_L \times U(1)_Y$ broke down to $U(1)_{EM}$ in this process. Since the $SU(2)_L \times U(1)_Y$ group has (3+1) generators i.e. 3 Pauli matrices as generators for $SU(2)_L$ and 1 identity matrix as generator for $U(1)_Y$. SSB thus generated masses for 3 gauge bosons (W^1_μ,W^2_μ,W^3_μ) leaving the B_μ to be massless. The kinetic part of the Lagrangian for these fields are,

$$\mathcal{L}_{Kinetic} = -\frac{1}{4} W^i_{\mu\nu} W^i_{\mu\nu} - \frac{1}{4} B_{\mu\nu} B_{\mu\nu}, \tag{2.13}$$

where,

$$W^i_{\mu\nu} = \partial_\mu W^i_\nu - \partial_\mu W^i_\nu + g\epsilon^{ijk} W^j_\mu W^k_\nu, \tag{2.14}$$

and

$$B_{\mu\nu} = \partial_\nu B_\mu - \partial_\mu B_\nu. \tag{2.15}$$

The charges of these groups present before and after the symmetry breaking are then constructed by Glashow to be,

$$Q = \tau_3 + \frac{Y}{2}, \tag{2.16}$$

where Q is the electric charge, τ_3 is the $SU(2)_L$ generator corresponding to the isospin and Y is the hypercharge.

2.3.1 Spontaneous Symmetry Breaking Through Higgs Mechanism

Symmetry conservation in any theory has two aspects:

1. The Lagrangian must remain invariant under the action of symmetry:

$$U(\theta)\mathcal{L}U^{\dagger}(\theta) = \mathcal{L}' = \mathcal{L}, \tag{2.17}$$

where *U(θ)* is the unitary matrix corresponding to the symmetry transformation.

2. Under the action of the symmetry transformation, the vacuum of the potential should remain invariant such that,

$$U(\theta)\left|0\right\rangle = \left|0\right\rangle. \tag{2.18}$$

In a case where the first condition is satisfied but the second condition is not, it means that the theory has a lagrangian that respects the symmetry, while it's ground state solution does not. This idea that the state does not need to have the same symmetry as the theory describes is known as Spontaneous Symmetry Breaking [45, 42]. The GWS model introduced SSB to generate masses for the gauge boson through the Higgs mechanism. We hence explain SSB in the context of the Higgs mechanism in the Standard Model below:

The main idea behind the Higgs Mechanism is the assumption of a new field, the Higgs field which has a non zero vacuum expectation value. While the non zero vev breaks the $U(1)_Y$ symmetry, a doublet representation of the Higgs field ensures that the $SU(2)_L$ symmetry is broken, while keeping the $U(1)_{EM}$ symmetry intact through charge assignment. The Lagrangian with the Higgs field Φ looks like,

$$\mathcal{L} = \mathcal{L}_{Fermion} + \mathcal{L}_{Boson} + (D_\mu\Phi)^{\dagger}(D_\mu\Phi) - \mu^2\Phi^{\dagger}\Phi - \lambda(\Phi^{\dagger}\Phi)^2. \tag{2.19}$$

where,

$$\Phi = \frac{1}{\sqrt{2}}\begin{pmatrix}\phi^+\\ \phi^0\end{pmatrix}, \tag{2.20}$$

and the covariant derivative D_μ is given as,

$$D_\mu = \partial_\mu - i\frac{g}{2}\tau^a_\mu W^a_\mu - i\frac{g'}{2}YB\mu, \tag{2.21}$$

where g and g' are the gauge couplings for the $SU(2)_L$ and $U(1)_Y$ group respectively.

The potential is then given as,

$$V(\Phi) = \mu^2\Phi^{\dagger}\Phi + \lambda(\Phi^{\dagger}\Phi)^2. \tag{2.22}$$

Now, if $\mu > 0$, the minima of this potential is found to be,

$$\Phi = \frac{1}{\sqrt{2}} \begin{pmatrix} 0 \\ v \end{pmatrix}. \tag{2.23}$$

But since important aspect of the Higgs field is that it has a negative parameter ($\mu < 0$) for its mass term, we have the potential minima (or the vev) to be at $v{=}\sqrt{-\frac{\mu^2}{\lambda}}$. Hence in the unitary gauge, the shifted Higgs field looks like,

$$\Phi = \frac{1}{\sqrt{2}} \begin{pmatrix} 0 \\ v + h \end{pmatrix}, \tag{2.24}$$

where h is the scalar higgs. To find the mass for the gauge bosons, one converts from the gauge basis to the mass basis through rotations and field redefinitions to get,

$$W_\mu^+ = \frac{1}{\sqrt{2}}(W_\mu^1 - iW_\mu^2), \tag{2.25}$$

$$W_\mu^- = \frac{1}{\sqrt{2}}(W_\mu^1 + iW_\mu^2), \tag{2.26}$$

$$Z_\mu^0 = -\, sin\theta_w B_\mu + cos\theta_w W_\mu^3, \tag{2.27}$$

$$A_\mu = cos\theta_w B_\mu + sin\theta_w W_\mu^3, \tag{2.28}$$

where the mixing angle θ_w is given by $\tan\theta = \frac{g'}{g}$ and the masses of the gauge bosons are,

$$m_W = \frac{1}{2} g v, \tag{2.29}$$

$$m_Z = \frac{1}{2}\sqrt{g^2 + g'^2}\, v = \frac{m_w}{cos\theta_w}, \tag{2.30}$$

$$m_A = 0. \tag{2.31}$$

This is how the Higgs mechanism successfully defines the mass for the vector bosons by expanding the Higgs field around an asymmetric vacua by giving it a non-zero vacuum expectation value. In Section 2.6 we see how this symmetry breaking event can be considered as a phase transition in a finite temperature background.

2.4 Effective Potential Formalism

This is a review on the calculation of finite temperature and first order loop corrections for the tree level field potential. It is inspired from lecture notes of the Summer School in HEP Cosmology at ICTP, [40].

2.4.1 Calculating the Effective Action

Using the path integral formalism, the generating functional (vacuum-to-vacuum amplitude) for a theory with scalar field ϕ is given as,

$$Z[j] = \int d\phi \exp\Big\{ i \int d^4x (\mathcal{L}\{\phi(x)\} + \phi(x) j(x)) \Big\} \tag{2.32}$$

Using this one can write the connected generating functional as,

$$Z[j] = \exp\big\{ iW[j] \big\}. \tag{2.33}$$

Now, the Legendre transform of Equation (2.33) becomes the effective action $\Gamma[\bar{\phi}]$ and is given as,

$$\Gamma[\bar{\phi}] = W[j] - \int d^4x \frac{\delta W[j]}{\delta j(x)} j(x), \tag{2.34}$$

where,

$$\bar{\phi} = \frac{\delta W[j]}{\delta j(x)}. \tag{2.35}$$

Now the effective action can be expanded in powers $\bar{\phi}$ as,

$$\Gamma[\bar{\phi}] = \sum_{n=0}^{\infty} \frac{1}{n!} \int d^4x .. d^4x_n \bar{\phi}(x_1) ... \bar{\phi}(x_n) \Gamma(x_1, ..., x_n), \tag{2.36}$$

where $\Gamma^{(n)}$ are the one-particle irreducible (1PI) Green functions. We now write the Fourier transform of $\Gamma^{(n)}$ and $\bar{\phi}$ to finally obtain the expression,

$$\Gamma[\bar{\phi}] = \sum_{n=0}^{\infty} \left[\frac{d^4p_i}{(2\pi)^4} \tilde{\phi}(-p_i) \right] (2\pi)^4 \delta^{(4)}(p_1 + ... + p_n) \Gamma^{(n)}(p_1, ..., p_n). \tag{2.37}$$

In a translationally invariant theory, the field $\bar{\phi}(x)$ is constant. Hence, we have,

$$\bar{\phi}(x) = \phi_c. \tag{2.38}$$

The effective potential $V_{\text{eff}}(\phi_c)$ is hence defined as,

$$\Gamma\big[\phi_c\big] = -\int d^4x V_{\text{eff}}(\phi_c). \tag{2.39}$$

Hence with the definition of the Dirac δ-function, we obtain the final expression,

$$V_{\text{eff}} = -\sum_{n=0}^{\infty} \frac{1}{n!} \phi_c^n \Gamma^{(n)}(p_i = 0). \tag{2.40}$$

Thus with the above calculation we infer that the effective action can be calculated in terms of 1PI diagrams. The universe is described by particles which interact at all loop levels. In QFT, we often follow the perturbative approach of calculating the potential upto the first few loop levels.

2.4.2 One Loop Effective Potential

In this thesis, we consider potentials which include interactions upto one loop. Hence we only consider 1 PI diagrams that contribute to 1 loop interactions (i.e. upto n=1 for Γ functions). We hence follow the formalism introduced by Weinberg and Coleman [15].

Scalar Fields

Let's consider the simplest form of the scalar field theory with the Lagrangian,

$$\mathcal{L} = \frac{1}{2}\partial^{\mu}\phi\partial_{\mu}\phi - V_0(\phi), \tag{2.41}$$

with a tree level potential,

$$V_0 = \frac{1}{2}m^2\phi^2 + \frac{\lambda}{4!}\phi^4. \tag{2.42}$$

From Figure 2.2, we see that the n-the diagram has n propagators, n vertices and 2n external legs. Following are their respective contributions:

1. n propagators: $i^n\big(p^2 - m^2 + i\epsilon\big)^{-n}$
2. External lines: ϕ_c^{2n}
3. Vertex factor : $-i\lambda/2$
4. Global symmetry factor: $\frac{1}{2n}$

Hence, from the rules described, we can now write the one-loop effective potential as,

$$V_{\text{eff}}(\phi_c) = V_0(\phi_c) + V_1(\phi_c), \tag{2.43}$$

with,

$$V_1(\phi_c) = i\sum_{n=1}^{\infty}\int\frac{d^4p}{(2\pi)^4}\frac{1}{2n}\left[\frac{\lambda\phi_c^2/2}{p^2 - m^2 + i\epsilon}\right]^n \tag{2.44}$$

$$= -\frac{i}{2}\int\frac{d^4p}{(2\pi)^4}log\left[1 - \frac{\lambda\phi_c^2/2}{p^2 - m^2 + i\epsilon}\right]. \tag{2.45}$$

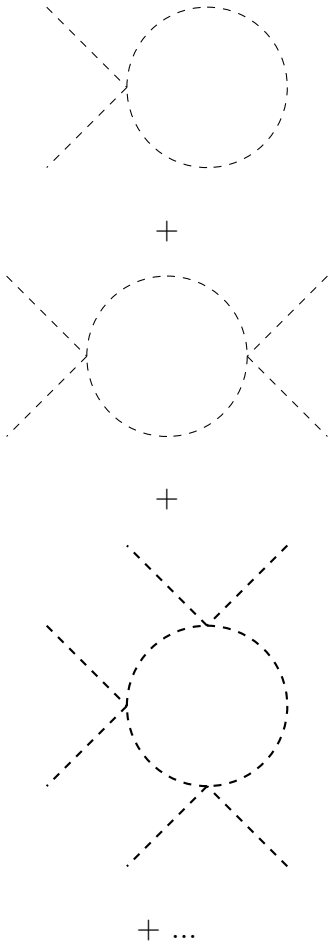

Fig. 2.2: 1PI diagrams for scalar fields that contribute to the one-loop effective potential.

Now, after Wick rotation $\left(p^0 = ip^0_E, p_E = (-ip^0, \vec{p})\right)$ and using the shifted mass,

$$m^2(\phi_c) = m^2 + \frac{1}{2}\lambda\phi_c^2 = \frac{\partial^2 V_0(\phi_c)}{\partial\phi_c^2}. \tag{2.46}$$

We finally get the complete 1 loop contribution to the effective potential as,

$$V_1(\phi_c) = \frac{1}{2}\int \frac{d^4p}{(2\pi)^4} log\big[p^2 + m^2(\phi_c)\big]. \tag{2.47}$$

Fermion Fields

In case of fermion of fields, we follow the similar procedure by starting with the lagrangian,

$$\mathcal{L} = i\bar{\psi}_a\gamma.\partial\psi^a - \bar{\psi}_a(M_f)^a_b\psi^b, \tag{2.48}$$

where the mass matrix $(M_f)^a_b\phi^i_c$ is a function of scalar fields linear in $\phi^i_c : (M_f)^a_b = \Gamma^a_{bi}\phi^i_c$.

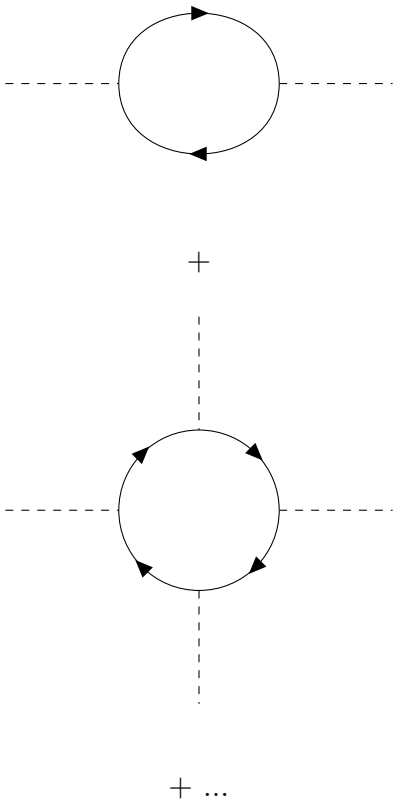

Fig. 2.3: 1PI diagrams for fermionic fields that contribute to the one-loop effective potential.

Now to calculate the contribution from the 1PI diagrams in Figure 2.3, we use the following rules,

1. 2n propagators: $Tr_s\big[i^2 n(\gamma.p)^{2n}(p^2+i\epsilon)^{-2n}\big]$
2. Vertex factor : $Tr\big[-i^{2n}M_f(\phi_c)^{2n}\big]$

Here, Tr_s indicates trace taken for all spinor indices s. Hence we finally get the total contribution,

$$-\frac{1}{2n}\frac{Tr(M_f^2 n)}{p^{2n}}2d, \tag{2.49}$$

where $2d$ refers to the number of degrees of freedom of fermion. For Dirac fermions it is $d=2$ and is $d=1$ for Weyl fermions. The overall minus sign comes from the fermion loop, while $\frac{1}{2n}$ is the combinatorial factor. Now we follow the procedure of Wick rotation similar to that done for the scalar potential. Leaving out the field independent terms, we finally get,

$$V_1 = -2d\frac{1}{2}Tr\int\frac{d^4p}{(2\pi)^4}log\big[p^2+M_f^2(\phi_c)\big]. \tag{2.50}$$

Gauge Boson Fields

An approach similar to the scalar and fermion fields is used for the Gauge boson case.

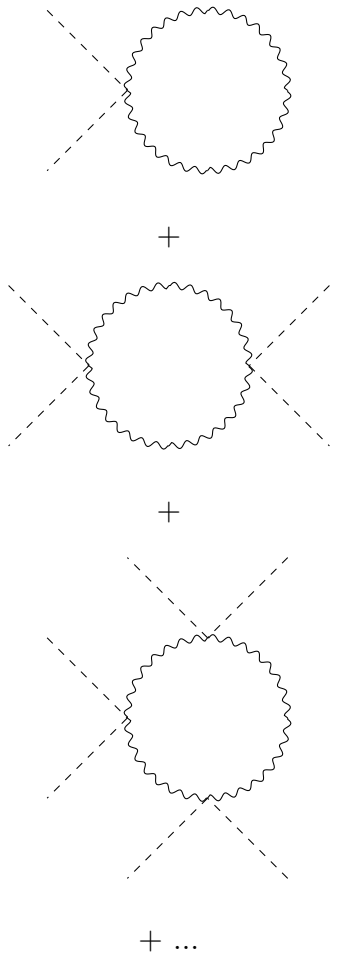

Fig. 2.4: 1PI diagrams for gauge fields that contribute to the one-loop effective potential.

We calculate the 1PI diagrams in Figure 2.4 and finally get,

$$V_1 = Tr(\Delta)\frac{1}{2}Tr\int\frac{d^4p}{(2\pi)^4}log\big[p^2+(M_g b)^2(\phi_c)\big], \tag{2.51}$$

where $Tr(\Delta)$ is the number of degrees of freedom and is equal to 3 for a massive gauge boson.

Renormalization

The final expressions for the one-loop effective potential obtained above in equations (2.51, 2.50 and 2.47) can be very well understood mathematically. However, we see that at infinite energies, they become divergent and hence lose their physical meaning. In order to correct for this UV-divergence, we follow the renormalization procedure. We

hence look at the following renormalization procedures:

Cut-off Regularization

In this procedure, we make our theory finite by introducing a cut-off momenta Λ. We start with the theory of a massless scalar field, with the Lagrangian,

$$\mathcal{L} = \frac{1}{2}(1+\delta Z)(\partial_\mu \phi)^2 - \frac{1}{2}\delta m^2 \phi^2 - \frac{\lambda + \delta\lambda}{4!}\phi^4, \tag{2.52}$$

where, δZ, δm^2 and $\delta\lambda$ are the usual wave-function, mass and coupling constant renormalization counter terms. Conventionally, for renormalized mass (m_R), renormalized four-point function coupling (λ) and field renormalization condition, we have,

$$m_R^2 = \left.\frac{d^2V}{d\phi_c^2}\right|_{\phi_c=0}, \tag{2.53}$$

$$\lambda_R = \left.\frac{d^4V}{d\phi_c^4}\right|_{\phi_c=0}, \tag{2.54}$$

$$Z(0) = 1. \tag{2.55}$$

We now use the cutoff momenta Λ and compute the integral in Equation (2.47), thus making the integral go from 0 to Λ^2. Hence neglecting terms that vanish as Λ approaches ∞ and other field independent terms, we get the one-loop contribution to the effective potential as,

$$V_1(\phi_c) = \frac{1}{32\pi^2} m^2(\phi_c)\Lambda^2 + \frac{1}{64\pi^2} m^4(\phi_c)\left[\log\frac{m^2(\phi_c)}{\Lambda^2} - \frac{1}{2}\right]. \tag{2.56}$$

Using the above equation, we have the total effective potential upto 1 loop as,

$$V = \frac{1}{2}\delta m^2\phi_c^2 + \frac{\lambda+\delta\lambda}{4!} + \frac{\lambda\phi_c^2}{64\pi^2}\Lambda^2 + \frac{\lambda^2\phi_c^4}{256\pi^2}\left(\log\frac{\lambda\phi_c^2}{2\Lambda^2} - \frac{1}{2}\right). \tag{2.57}$$

In our theory, the renormalization conditions are hence given as,

$$\frac{d^2V}{d\phi_c^2}|_{\phi_c=0} = 0, \tag{2.58}$$

$$\frac{d^4V}{d\phi_c^4}|_{\phi_c=\mu} = \lambda, \tag{2.59}$$

$$Z(0) = 1. \tag{2.60}$$

Where μ is a mass scale. Finally we impose the renormalization conditions on the total effective potential in Equation (2.57) to calculate the values of δZ, δm^2 and $\delta\lambda$. Thus,

substituting these values, we arrive at the renormalized one-loop effective potential for our scalar field theories as,

$$V_{\text{eff}} = \frac{\lambda}{4!}\phi_c^4 + \frac{\lambda^2\phi_c^4}{256\pi^2}\log\left(\frac{\phi_c^2}{\mu^2} - \frac{25}{6}\right). \tag{2.61}$$

Similarly, we can also renormalize the fermion fields. To renormalize gauge bosons without explicitly breaking the gauge invariance, we adopt the procedure of dimensional regularisation.

Dimensional Regularisation

This method involves making a clever redefinition of the dimension dependent powers of the integrant and solve the integral such that the divergences in the theory vanish. The method of $\bar{MS}$ renormalization is vastly used in the calculation of effective potential. In this method, we write the one loop correction as,

$$V_1(\phi_c) = \frac{1}{2}(\mu^2)^{2-n}\int \frac{d^n p}{(2\pi)^n}\log\left[p^2 + m^2(\phi_c)\right]. \tag{2.62}$$

Where μ is a scale with mass dimension which needs to be introduced to balance the integration measure. Thus we differentiate the potential V with respect to $m^2(\phi_c)$ to get V' as,

$$V' = \frac{1}{2}(\mu^2)^{2-n}\int \frac{d^n p}{(2\pi)^n}\frac{1}{p^2 + m^2(\phi_c)}. \tag{2.63}$$

We now use the standard formula of dimensional regularization and write the integral in the above equation in terms of Gamma functions. We then integrate the Equation (2.63) again with respect to $m^2(\phi_c)$ to get V_1. To solve it further, we expand the gamma function term $\Gamma(2-\frac{n}{2})$ in powers of 2-n/2 and absorb the divergent terms by counterterms. Hence the final correction term for the one-loop renormalized scalar field theory is,

$$V_1(\phi_c) = \frac{1}{64\pi^2}m^4(\phi_c)\log\left\{\frac{m^2(\phi_c)}{\mu^2} - \frac{3}{2}\right\}. \tag{2.64}$$

Similarly, for fermions we obtain,

$$V_1(\phi_c) = -d\frac{1}{32\pi^2}M_f^4(\phi_c)\log\left\{\frac{M_f^2(\phi_c)}{\mu^2} - \frac{3}{2}\right\}, \tag{2.65}$$

and for gauge bosons, the gauge invariant one loop renormalized correction is given as,

$$V_1(\phi_c) = 3\frac{1}{64\pi^2}M_{gb}^4(\phi_c)\log\left\{\frac{M_{gb}^2(\phi_c)}{\mu^2} - \frac{5}{6}\right\}. \tag{2.66}$$

Thermal corrections

In order to account for the *real* potential of the hot universe, the temperature dependence of the interaction between the particles needs to be considered. We hence use the imaginary time formalism, with Feynman rules as follows,

1. Boson propagator: $\frac{i}{p^2-m^2}; p^\mu = [2ni\pi\beta^{-1}, \vec{p}]$
2. Fermion Propagator: $\frac{i}{\gamma.p-m}; p^\mu = [(2n+1)i\pi\beta^{-1}, \vec{p}]$
3. Loop integral : $\frac{i}{\beta}\sum_{n=-\infty}^{\infty}\int\frac{d^3p}{(2\pi)^3}$
4. Vertex Function: $-i\beta(2\pi)^3\delta(\sum w_i)\delta^3(\sum\vec{p}_i)$

Using the above rules, the Equation (2.47) is calculated as,

$$V_1^\beta(\phi_c) = \frac{1}{2\beta}\sum_{n=-\infty}^{\infty}\int\frac{d^3p}{(2\pi)^3}\log(w_n^2+w^2), \tag{2.67}$$

where w_n are the bosonic Matsubara frequencies and,

$$w^2 = \vec{p}^2 + m^2(\phi_c), \tag{2.68}$$

where m is the mass of the scalar field and p is the momentum of the field. Now, in the Equation (2.67) the sum over n diverges but the infinite part does not depend on ϕ_c. We hence define the quantity,

$$v(w) = \sum_{n=-\infty}^{\infty}\log(w_n^2+w^2). \tag{2.69}$$

With the clever use of certain identities the above equation can be written as,

$$v(w) = 2\beta\left[\frac{w}{2}+\frac{1}{\beta}\log(1-e^{-\beta w})\right] + w - \text{independent terms.} \tag{2.70}$$

Thus we use the above equation in equation(2.67) using equation(2.70) to get,

$$V_1^\beta(\phi_c) = \int\frac{d^3p}{(2\pi)^3}\left[\frac{w}{2}+\frac{1}{\beta}\log(1-e^{-\beta w})\right]. \tag{2.71}$$

At zero temperature, the above equation is calculated to be merely the one-loop effective potential calculated in Equation (2.47). One can further simplify the temperature dependent part by using the Residue theorem and performing Wick rotation.

$$\frac{1}{\beta}\int\frac{d^3p}{(2\pi)^3}\log\left(1-e^{-\beta w}\right) = \frac{1}{2\pi^2\beta^4}J_B[m^2(\phi_c)\beta^2], \tag{2.72}$$

where, J_B is the thermal bosonic function defined as,

$$J_B[m^2\beta^2] = \int_0^\infty dx x^2 \log\left[1 - e^{-\sqrt{x^2+\beta^2 m^2}}\right]. \tag{2.73}$$

In `CosmoTransitions` [43], we input all the above derived relations and the potential V_o. It has an inbuilt function to calculate the finite temperature one loop corrections using the user defined fields in the model. As derived above, 1 loop finite temperature corrections are calculated using, [40],

$$V_1^\beta(\phi, T) = \int \frac{d^3p}{(2\pi)^3}\frac{w}{2} + \frac{T^4}{(2\pi)^2} J_B\left(\frac{m(\phi_i)^2}{T^2}\right), \tag{2.74}$$

where $m(\phi_i)$ is the mass of field ϕ_i within the theory. The function J_B brings in temperature dependent corrections and is given as [40] to calculate the corrections and uses all the fields defined. Since we know that the maximum contributions to one loop corrections come from the contribution of W, Z bosons and the top quark, these fields are introduced in our code along with their usual degree of freedom and Higgs dependent masses.

2.5 Electroweak Phase Transitions

As the universe cools down, the effective potential changes due the presence of temperature dependent terms as derived in Section 2.4. The process of a phase transition (PT) involves an energetically favourable transition from the initial vacuum state of the universe to another, as the universe cools. These PTs can be of two types: (1)Second Order PTs- occur via a smooth (crossover) transition from the old vacuum to the new one. Because this transition is not turbulent, no GWs are produced. (2)First Order PTs- require quantum tunneling across the barrier between the two vacuum states. Such PTs occur through the formation of bubbles of new phase in the background of the old phase. In this section we discuss these two PTs in brief:

2.5.1 Second Order Phase Transition

As the temperature of the universe varies, the structure of the potential varies along with it. However, for the potential in Equation (2.75) it is seen that there is a smooth transition between the initial and the global minima. This is the case in Second Order Phase Transitions.

To make the discussion lucid, we start with a generic temperature dependent potential

with a scalar field ϕ,

$$V(\phi, T) = A(T^2 - T_0^2)\phi^2 + \frac{\Delta(T)}{4}\phi^4, \tag{2.75}$$

where A is a constant independent of temperature T and $\Delta(T)$ is some function of T.

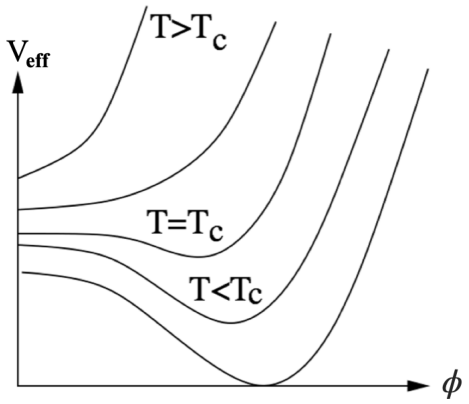

Fig. 2.5: Temperature dependent potential in case of second order phase transitions.

On minimizing this potential, we get two stationary points,

$$\phi = 0, \tag{2.76}$$

$$\phi = \sqrt{\frac{2A(T_0^2 - T^2)}{\Delta(T)}}. \tag{2.77}$$

Now consider that this system cools from very high temperatures just like our universe. When $T > T_0$, the stationary point in Equation (2.77), becomes imaginary and hence only one real stationary point which is a minima in this case as $\frac{\partial^2 V}{\partial \phi^2} > 0$. As the temperature cools further, both the above stationary points coincide at $\phi = 0$. At even lower temperatures when $T < T_0$, we find that $\phi = \sqrt{\frac{2A(T_0^2 - T^2)}{\Delta(T)}}$ becomes the global minima ($\frac{\partial^2 V}{\partial \phi^2} > 0$) while $\phi = 0$ becomes the maxima($\frac{\partial^2 V}{\partial \phi^2} < 0$). This is how the potential minima changes with changing temperature. For this type of potential with only quadratic and quartic terms in ϕ, we see no barrier between the initial and final minima in Figure 2.5. Such type of a smooth phase transition is called the second order phase transition.

2.5.2 First Order Phase Transition

As the temperature of the universe varies, the structure of the potential varies along with it. In presence of cubic field terms as in Equation (2.78), the potential forms a barrier between the two minima, leading to a First Order Phase Transition.
In case we include a cubic term in our potential, we then have,

$$V(\phi, T) = A(T^2 - T_0^2)\phi^2 - DT\phi^3 + \frac{\lambda}{4}\phi^4, \tag{2.78}$$

where A, D and λ are functions independent of T.

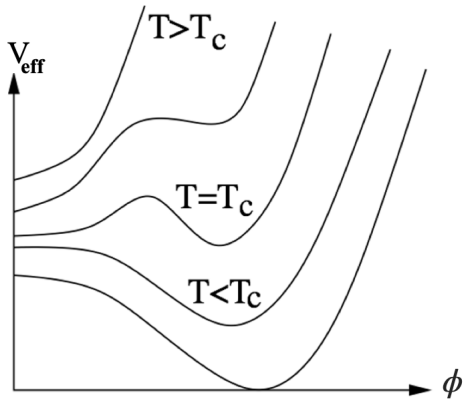

Fig. 2.6: Temperature dependent potential in case of first order phase transitions.

At high temperatures, the potential has only one minimum at $\phi = 0$ at $T > T_h$ where,

$$T_h = \sqrt{\frac{8\lambda A T_0^2}{(8\lambda A - 9D^2)}}, \tag{2.79}$$

As the temperature becomes T_h, a local minima arises at,

$$\phi(T_h) = \frac{3AT_h}{2\lambda}. \tag{2.80}$$

When the systems cools even further, the temperature goes below T_h. In this case, a barrier is seen to be formed between the two minima at $\phi = 0$ and $\phi \neq 0$. As the temperature lowers further, the minima at $\phi \neq 0$ then splits at,

$$\phi = \frac{3AT_h}{2\lambda} - \frac{\sqrt{9D^2T^2 - 8\lambda A(T^2 - T_0^2)}}{2\lambda}, \tag{2.81}$$

to be a maxima and at,

$$\phi = \frac{3AT_h}{2\lambda} + \frac{\sqrt{9D^2T^2 - 8\lambda A(T^2 - T_0^2)}}{2\lambda}, \tag{2.82}$$

to be a minima. As the temperature lowers, there is a specific temperature at which the the two minima become degenerate. This temperature is called the critical temperature (T_c) and is characteristic of any phase transition. For our potential, it is given as,

$$T_c = \sqrt{\frac{\lambda A T_0^2}{\lambda A - D^2}}. \tag{2.83}$$

When the temperature goes below T_c, the minima at $\phi = 0$ becomes metastable while the

minima at $\phi \neq 0$ becomes stable. At a specific temperature $T = T_0$, the former minima converts to a maxima as shown in Figure 2.6.

Since there is a potential barrier between the initial and final minima, first order phase transitions occur via tunneling through the barrier from one phase to the other. However if the barrier is too high then the tunneling takes place at a lower temperature T such that $T_c > T > T_0$. The barrier penetration through thermal tunneling is the signature of a FOPT. The important difference between (2.78) and (2.75) is that the former one contains terms that are cubic in the field ϕ, which are hence responsible for causing the FOPT.[1]

Bubble Dynamics

FOPTs occur through the formation of bubbles of new phase(true vacuum) in the background of the old phase(false vacuum). As the universe cools and approaches the critical temperature, both the phases are equally energetically favourable. For temperatures below T_c, the new minima at $\phi \neq 0$ becomes the global minima or the true vacuum. Hence a transition from the older minima to this global minima becomes energetically favourable.

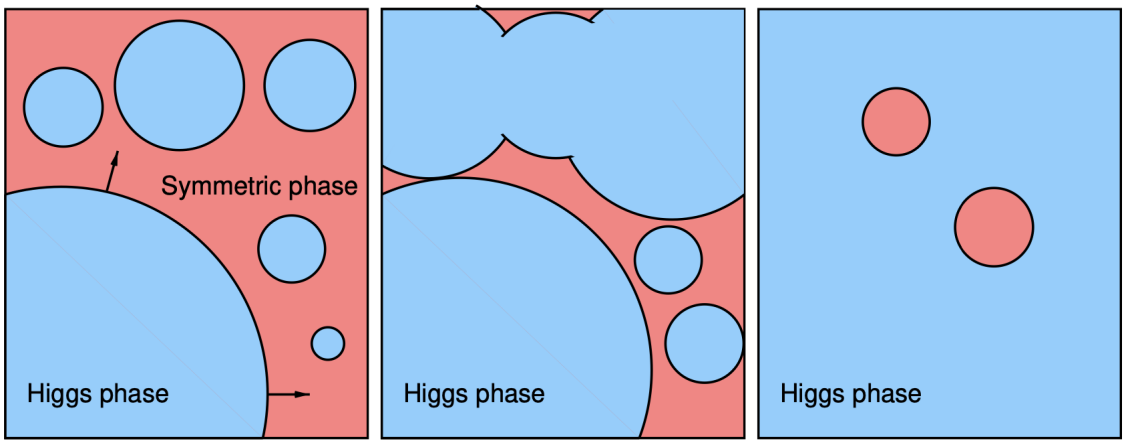

Fig. 2.7: Bubbles of new/Higgs phase (true vacuum) form, expand and merge in the background of the old phase (false vacuum) such that by the end of the First Order Phase transition, the whole universe is in the true vacuum [26].

Thus, the rate of tunneling for a field ϕ at temperature T is,

$$\Gamma \propto e^{-\frac{F_c(T)}{T}}, \tag{2.84}$$

where $F_c(T)$ is the surplus free energy needed to create a bubble of true vacuum large enough to grow indefinitely. However, the nucleation of bubble does not start until and

[1] We do not consider higher order terms of ϕ beyond the quartic ones because such terms are not renormalizable in a four-dimensional theory by power counting.

unless the rate of tunneling exceeds the Hubble expansion rate. This condition can be achieved when the euclidean action $S(T) \approx \frac{F_c}{T}$ corresponding to the bounce solution in (2.86) becomes $O(130-140)$. This ensures that at least one critical bubble is nucleated per unit Hubble volume and the corresponding temperature is known as the nucleation temperature (T_{nuc}). The surplus energy for a true vacuum bubble is,

$$F = \int d^3x \left\{ \frac{1}{2}(\nabla\phi)^2 + V_{\text{eff}}(\phi, T) \right\}, \tag{2.85}$$

where V_{eff} is the effective potential.
The symmetrical symmetry of the bubbles at very high temperatures causes the scalar field to obey the following equation of motion,

$$\frac{\partial^2\phi}{\partial r^2} + \frac{2}{r}\frac{\partial\phi}{\partial r} = \frac{\partial V(\phi, T)}{\partial\phi}, \tag{2.86}$$

along with boundary conditions,

$$\lim_{\phi\to\infty} \phi(r) = 0 \quad \text{and} \quad \left.\frac{\partial\phi}{\partial r}\right|_{r=0} = 0. \tag{2.87}$$

The solution of Equation (2.86) corresponds to the continuous evolution of the field from false vacuum to true vacuum and is known as bounce solution. Incorporating this symmetry in our Euclidian action/ surplus free energy, we have,

$$F = \int d^3x \left\{ \frac{1}{2}\left(\frac{\partial\phi}{\partial r}\right)^2 + V_{\text{eff}}(\phi, T) \right\}, \tag{2.88}$$

The free energy of bubbles is distributed into two parts [1]: (1) Surface energy term coming from the derivative term in (2.86) and (2) Volume term arising from the difference in free energy density inside and outside the bubble. While the bubbles can be either thick or thin walled, the first bubble formed just after temperature dips below T_c, is always thin walled. In general, the thickness of the bubble wall depends on how large the rate of tunnelling (2.84) becomes before thick walled bubbles are energetically preferred [1]. Thus for a first order phase transition to take place, bubbles necessarily need to occupy most of the space before the temperature drops to T_0.

Phase Transition Parameters

Having briefly described the bubble dymanics above, we now define two important parameters useful to understand first order phase transitions:

1. **Nucleation Rate (β)**- The inverse of nucleation rate β is the time required to complete the phase transition. Nucleation rate is defined as [22],

$$\beta = H_{\text{nuc}} T_{\text{nuc}} \left.\frac{dF_c}{dT}\right|_{T_{\text{nuc}}}, \tag{2.89}$$

where H_{nuc} is the Hubble rate at T_{nuc} and corresponds to physical units of energy time. It can be calculated using its redshift(z) dependent form from Friedmann equations as given in [18]. We further use the CMB (Cosmic Microwave Background) based relation of temperature dependence of z given as $T = 2.78(1+z)$, [13]. To calculate the nucleation rate in `CosmoTransitions`, we use an approximate formula given in [25],

$$\frac{\beta}{H_{\text{nuc}}} = \frac{S(t_{\text{nuc}})}{1 - T_{\text{nuc}}/T_c}, \tag{2.90}$$

where $S(t_{\text{nuc}})$ is the value of the action calculated at the time when the nucleation temperature is achieved. This quantity is calculated by `CosmoTransitions` using the approximations mentioned in Section 2.5.2.

2. **Latent Heat Fraction (α)**- During a first order PT, as the system moves from a high temperature phase to a low temperature phase, it stores some energy in the form of heat. This energy is then released through bubble expansion. We have,

$$\alpha = \left.\frac{\rho_{\text{vac}}}{\rho_{\text{rad}}}\right|_{T_{\text{nuc}}}, \tag{2.91}$$

where ρ_{vac} is the vacuum energy released in PT given by,

$$\rho_{\text{vac}} = \frac{\pi g^*}{30} T_{\text{nuc}}^4, \tag{2.92}$$

and ρ_{rad} is the total radiation density given as [25, 27],

$$\rho_{\text{rad}} = \left.\left[V - T_{\text{nuc}} \frac{\partial V}{\partial T}\right]\right|_{\text{symmetric}} - \left.\left[V - T_{\text{nuc}} \frac{\partial V}{\partial T}\right]\right|_{\text{asymmetric}}, \tag{2.93}$$

where g*=106.75 denotes the relativistic degrees of freedom [10, 9, 22].

In Chapter 3, we discuss how these bubbles lead to the formation of primordial gravitational waves.

2.6 Electroweak Phase Transitions in the Standard model

For a universe completely described by the standard model, we expect a phase transition to have occurred during the electroweak era as the electroweak symmetry broke from $SU(2)_L \times U(1)_Y$ to $U(1)_{EM}$ as described previously in Section 2.3.1. For our discussion in this context, we now can consider gauge bosons from the GWS theory to calculate the phase transition parameters as follows.

We start with the Higgs scalar doublet field Φ, which after SSB is given as,

$$\Phi = \frac{1}{\sqrt{2}} \begin{pmatrix} \chi_1 + i\chi_2 \\ \phi + h + i\chi_3 \end{pmatrix}, \tag{2.94}$$

where $\chi_i s$ are the Goldstone bosons and ϕ is the real constant background. Now after inserting this into the potential (2.42), we get the field dependent masses of the scalar field as,

$$m_h^2(\phi) = 3\lambda\phi^2 - m^2, \tag{2.95}$$

$$m_\chi^2(\phi) = \lambda\phi^2 - m^2. \tag{2.96}$$

A common way to mention the masses of gauge bosons is by saying that these gauge bosons eat up the Goldstone bosons to get field dependent masses given by,

$$m_W^2(\phi) = \frac{g^2}{4}\phi^2 \quad \text{and} \quad m_Z^2(\phi) = \frac{g^2 + g'^2}{4}\phi^2, \tag{2.97}$$

and the most dominant fermionic contribution comes from the top quark mass given as,

$$m_t^2(\phi) = \frac{y_t^2}{2}\phi^2, \tag{2.98}$$

where y_t is the Yukawa coupling constant of top quark. To calculate the phase transition, we use the zero temperature one loop potential given in (2.64), (2.65) and (2.66) and use the field dependent masses to calculate the finite temperature potential correction (2.74). The degrees of freedom of different particles used in calculating the zero temperature one loop potential are given as,

$$d_h = 1, d_\chi = 3, d_W = 6, d_Z = 3, d_t = 12. \tag{2.99}$$

Specifically, we see that the finite temperature effective potential is approximated by Equation (2.78),

$$V(\phi, T) = A(T^2 - T_0^2)\phi^2 - DT\phi^3 + \frac{\lambda}{4}\phi^4, \tag{2.100}$$

where,

$$A = \frac{g^2 + 3g'^2 + 4y_t^2 + 8\lambda}{32}, \tag{2.101}$$

$$D = \frac{2g^3 + (g'^2 + g'^2)^{3/2}\lambda}{32\pi}, \tag{2.102}$$

$$T_0 = \frac{m_h^2}{4A}. \tag{2.103}$$

Clearly, since this potential is similar to that discussed in Section 2.5.2, we expect that as the temperature lowers, we see a minima appear at $\phi \neq 0$, and further below that temperature a barrier is formed between the two minima. Hence this type of potential can cause a FOPT. In case of the SM, the critical temperature using Equation (2.83) and the values of the constant A, D and T_0 given above, is calculated to be,

$$T_c = \frac{8m_h^2}{(g^2 + 3g'^2 + 4y_t^2 + 8\lambda)}\left(1 - \frac{(2g^3 + (g'^2 + g'^2)^{3/2}\lambda)^2}{32\lambda\pi^2(g^2 + 3g'^2 + 4y_t^2 + 8\lambda)}\right)^{-1/2}. \tag{2.104}$$

From the above equations, it is important to note that while the potential has a cubic term which is favourable for a FOPT, the critical temperature depends on the mass of the Higgs, Yukawa and the gauge coupling constants. This means that the strength of the phase transition depends on all these constant factors. It is important to note that the above calculation is valid only when the coupling strength between the particles is ≈ 1. Instead, if it is greater than 1, our perturbative thermal calculations break down and one requires a detailed calculation using lattice simulations in such a non-perturbative regime.

In general, we can study the EWPT in a two dimensional space spanned by temperature and the ratio of the Higgs mass to the mass of the gauge boson. As long as the ratio of Higgs mass to the mass of gauge boson is small, the perturbative calculation done above is valid and the phase transition indeed turns out to be first order in nature. Now given that we already know the gauge boson mass to be $\approx$ 80 GeV , the determining factor remains the (now recently observed) Higgs mass. For the Standard Model, if this Higgs mass was 80 GeV, a FOPT would be possible. As this Higgs mass increases, the ratio of Higgs mass to the mass of gauge boson increases and this reduces the strength of the FOPT. After a certain critical value of this Higgs mass to gauge boson mass ratio, a smooth crossover transition takes place as seen in Figure 2.6 for temperatures below the critical temperature. Given that the recently observed Higgs boson mass of 125 GeV

brings this ratio well beyond the critical ratio value, we say that the SM predicts the electroweak PT to be a crossover transition.

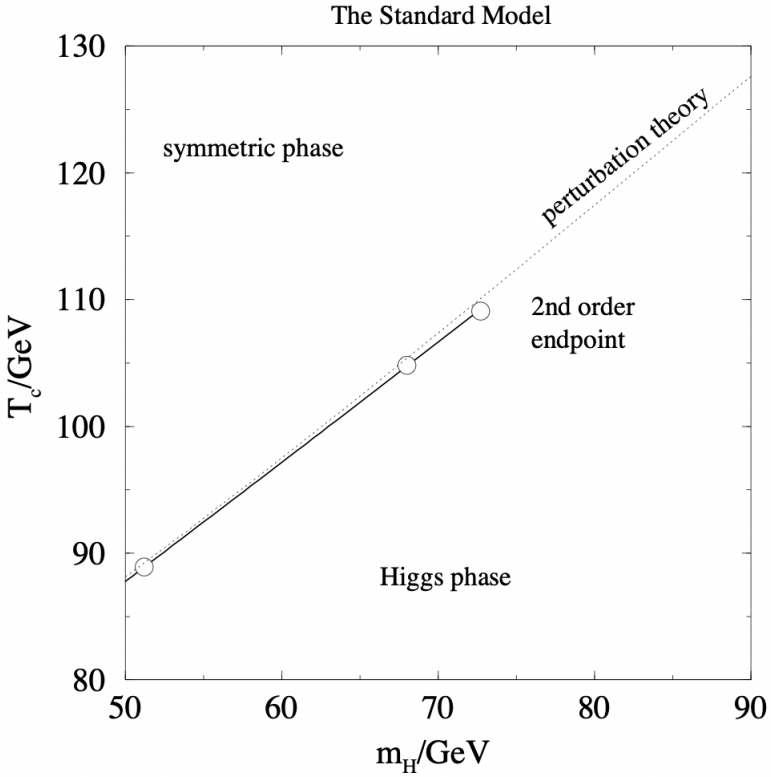

Fig. 2.8: The phase diagram of the Standard Model as studied by 3D as well as 4D simulations.

The theory in the perturbative regime always undergoes a First order phase transition. The strength of this transition reduces with increasing Higgs mass and ends around $m_H = 80$GeV (end-point) beyond which it enters the non perturbative region, [35].

Crossover Transition

Crossover transitions occur when the ground state of the system changes radically in the non-perturbative regime (any perturbative expansion around the original ground state would fail to capture the new ground state). In spite of a drastic phase change, no discontinuities are present in the derivatives (at any order whatsoever) of the free energy functional (such discontinuities are a characteristic of phase transitions), which is why crossover transitions do not actually come under the umbrella term of *canonical phase transitions*. Due to the absence of these discontinuities, they are 'smooth' transitions somewhat similar to second order phase transitions (which have a discontinuous second order derivative but a continuous first order derivative of free energy) and hence they are often confused with each other.

3. GRAVITATIONAL WAVES FROM FIRST ORDER PHASE TRANSITIONS

3.1 Introduction

In 1915, Einstein published *The General Theory of Relativity*, where he first theoretically predicted the existence of gravitational waves, however believing that detecting such miniscule oscillations was beyond the technological reach of mankind. However, 100 years later, the Laser Interferometer Gravitational Wave Observatory (LIGO) made history by successfully detecting gravitational waves caused by the merger of two compact objects. Ever since then, gravitational waves have been studied extensively as one can infer crucial information about their source by studying the observed signals. In the next decade, LISA, a space based interferometer will be in operation to detect GWs in the milliHertz range($10^{-4} - 10^{-2}$), thus making a strong case for detecting primordial gravitational waves formed around 200-100 GeV i.e. from electroweak PT era. Generally, GWs can be divided into two types: (1) Astrophysical Gravitational waves- formed by the dynamics between astrophysical objects and (2) Primordial Gravitational Waves- caused by turbulent cosmological processes in the early universe.

In this section, we discuss the formation of primordial gravitational waves as perturbation in the 4D space-time of the universe using the General Relativity(GR) formalism. We then discuss these gravitational waves in the context of First Order Phase transitions by describing the possible sources and their respective signal spectra that we expect to observe.

3.2 Gravitational Radiation

The following review is adapted from Maleknejad's lecture notes on Cosmological Gravitational Waves [36].

In general, Einstein's field equations are non-linear and have solutions that are difficult to obtain. Hence, shortly after proposing the general theory of relativity, Einstein proposed

linearized gravity in the form of small perturbations in the spacetime metric given as,

$$g_{\mu\nu} = \eta_{\mu\nu} + h_{\mu\nu}(\vec{x}), \tag{3.1}$$

in which $h_{\mu\nu}(\vec{x})$ and all its partial derivatives are small. The region where the metric takes this form describes a region of spacetime which is weakly curved i.e. the presence of a weak gravitational field. Now the Einstein tensor can be written in terms of the Ricci tensor $R_{\mu\nu} \equiv R^{\gamma}_{\mu\gamma\nu}$ and the curvature tensor $R \equiv R^{\mu}_{\mu}$, both of which contain derivatives of the metric such that,

$$G_{\mu\nu} = R_{\mu\nu} - \frac{1}{2} g_{\mu\nu} R = 8\pi G T_{\mu\nu}, \tag{3.2}$$

Now, inserting the weak field metric (3.1) in the above equation and calculating the Ricci and the curvature tensor we get,

$$\partial_\alpha \partial^\alpha h_{\mu\nu} + \partial_\mu \partial_\nu h - \partial_\nu \partial_\lambda h^\lambda_\mu - \partial_\mu \partial_\lambda h^\lambda_\nu - \eta_{\mu\nu}(\partial_\alpha \partial^\alpha h - \partial_\sigma \partial^\lambda h^\lambda \sigma) = -16\pi G T_{\mu\nu}, \tag{3.3}$$

where h is the trace of the field, $h \equiv h^{\mu}_{\mu}$. One can then use the field redefinition,

$$\tilde{h}_{\mu\nu} = h_{\mu\nu} - \frac{1}{2}\eta_{\mu\nu} h, \tag{3.4}$$

which is the trace reverse cousin of $\tilde{h} = -h$. Now since these fields are defined only upto gauge transformations , one conveniently uses the Lorenz gauge, $\partial_\mu \tilde{h}^{\mu\nu} = 0$. Hence finally the simple form is given as,

$$\partial_\alpha \partial^\alpha \tilde{h}_{\mu\nu} = -16\pi G T_{\mu\nu}. \tag{3.5}$$

In a completely empty universe, $T_{\mu\nu} = 0$ and the above Equation (3.5) has plane wave solutions with null wave vectors.

In presence of a source with non-zero $T_{\mu\nu}$, we need to solve the Equation (3.5) using Green's equation,

$$\partial_\alpha \partial^\alpha G(x^\mu - y^\mu) = \delta^4(x^\mu - y^\mu), \tag{3.6}$$

where the required retarded Green's function for $x^0 > y^0$ is,

$$G(x^\mu - y^\mu) = \frac{1}{(4\pi)|\vec{x} - \vec{y}|} \delta(x^0 - y^0 - |\vec{x} - \vec{y}|) \tag{3.7}$$

Therefore, the solution of the linearized gravitational equation in presence of a source is,

$$\tilde{h}_{\mu\nu}(\vec{x}, t) = -\frac{4G}{c^2} \int d^3y \frac{T_{\mu\nu}(\vec{y}, ct - |\vec{x} - \vec{y}|)}{|\vec{x} - \vec{y}|}. \tag{3.8}$$

Hence it has now become clear that the energy momentum tensor $T_{\mu\nu}$ governs the grav-

itational wave by acting a weak field perturbation source term in the metric. Further, to exhaust all degrees of freedom, one goes into the traceless-transverse gauge and identifies only the components of $\tilde{h}_{\mu\nu}$ in this gauge to be gravitational radiation. Equation (3.8) can be further approximated to be in a simpler form of the nature of quadrupole moments, however this approximation is *only* valid for compact sources (with very small spatial sizes as compared to the distance to the point of observation) for gravitational radiation as in the case for astrophysical GWs. Such an 'approximation is called the far field approximation' [36]. However since primordial GWs are hypothesized to have formed at every point in the universe, this approximation cannot be applied and then one should consider all terms in the Taylor expansion of $\frac{1}{\vec{x}-\vec{y}}$.

3.3 Sources of Gravitational Waves

Even though gravitational waves can propagate in an almost empty universe like ours, it needs a massive source for GW production. In Section 3.2, we saw that the linearized Einstein field equations have a source term $T_{\mu\nu}$, which is exactly what gives rise to gravitational radiation. The three primary sources of GWs (contributions to the total energy-momentum tensor) from the First order PTs are given below.

3.3.1 Bubble Collisions

During a first order phase transition, bubbles of true vacuum (broken symmetry phase) are created in a background of false vacuum. As spherically symmetric bubble has zero quadrupole or higher order moments, it cannot create gravitational waves. However, bubble collisions break this spherical symmetry of the Higgs fields and hence give rise to gravitational radiation [37, 28]. These gravitational waves receive energy from the kinetic energy stored in the Higgs field and the bulk motion of the plasma.

$$T_{\mu\nu} = d_\mu\phi d_\nu\phi - g_{\mu\nu}\left(\frac{d_\eta\phi d^\eta\phi}{2} - V_o\right), \tag{3.9}$$

where V_o is the field dependent tree level potential.

An important approximation used for numerically simulating multiple bubble collisions is the 'envelope approximation'. It states that a fraction κ of the latent heat of phase transition is confined in an infinitely thin shell near the PT front. This can be mathematically described in terms of two approximations- first, that the stress energy tensor is non zero only in an infinitesimal region at the bubble wall and the second is that the

stress energy tensor vanishes when the bubbles have overlapped [28]. Hence, once a shell collides with other, the energy stored in that shell dissipates quickly.

3.3.2 Sound Waves

As the bubble expands in hot plasma, the bubble wall experiences pressure and friction from the plasma outside it. This causes energy to dissipate to the external plasma. The excess energy received from the bubble walls now causes perturbations and subsequently sound waves in the plasma.

This can also be approximated in terms of a fluid v_μ of surrounding plasma particles as it is easier to then account for the plasma interactions inside, outside and on the bubble wall in terms of fluid pressure [44]. After collisions, as the domain walls disappear, primarily compressive fluid perturbations are left behind [25]. Sound waves are hence formed as a result of rarefaction and compression waves formed as the bubbles expand and merge. These perturbations cause sheer stress in the system which leads to the formation of gravitational waves. The stress energy tensor from the sound contribution is

$$T_{\mu\nu} = U v_\mu v_\nu - p g_{\mu\nu}, \tag{3.10}$$

where U is the enthalpy of the fluid and p is the pressure. The sound contribution is generally more prevalent than that due to bubble collisions in the formation of gravitational radiation.

3.3.3 Magnetohydrodynamic Turbulence

Magnetohydrodynamic(MHD) turbulence comes into picture if there exists a magnetic field during the electroweak PT. There are certain models [29] that describe MHD turbulence as a consequence of bubble collisions. When two bubbles collide, magnetic field is produced in the plasma. Together with the collision shock wave, this causes a turbulence in the magnetic field. This turbulence leads to redistribution of energy between the fluid and the field. In such a scenario, the fluid is ionised and this redistributed energy then gives rise to GWs. The stochastic nature of GWs becomes very clear as we consider multiple bubble collisions throughout spacetime. The spatial part of the stress energy tensor is

$$T_{ij}(x,\tau) = \frac{4\pi}{3}\rho_\tau v_i(x,\tau) v_j(x,\tau), \tag{3.11}$$

where τ is the conformal time, v_i and v_js are the velocities of the turbulent flow and ρ is the thermal energy density of the universe. MHD turbulence has a sub-dominant contribution towards gravitational radiation.

3.4 Gravitational Wave Energy Density Parameter

In this section, we discuss how the above described gravitational wave sources contribute to the total gravitational wave energy density parameter that we expect to observe.

Contribution from Bubble Collisions

Using the envelope approximation discussed in Section 3.3.1 the bubble wall velocity v_b can be scaled as a function of the latent heat α as [30],

$$v_b(\alpha) = \frac{0.577 + \sqrt{\alpha^2 + 0.66\alpha}}{1 + \alpha}. \tag{3.12}$$

We can hence write the peak frequency of f^* the GW energy density parameter at Hubble time as,

$$f^* = \left(\frac{0.62}{1.8 - 0.1v_b + v_b^2}\right)\beta. \tag{3.13}$$

The redshifted peak frequency is then given by [28],

$$f_{\text{col}} = \left(\frac{f^*}{\beta}\right)\left(\frac{T_*}{100GeV}\right)\left(\frac{H_*}{\beta}\right)^{-1}\left(\frac{g_*}{100}\right)^{1/6} \times 16.5 \times 10^{-6}\text{Hz}, \tag{3.14}$$

where H_* and T_* are the Hubble rate and the temperature at the phase transition respectively. Now we define the quantity $S_{\text{col}}(f)$ corresponding to the spectral shape parametrisation of the GW and the fitted form of the simulation data. It is hence given as [28],

$$S_{\text{col}}(f) = \frac{3.8(f/f_{\text{col}})^{2.8}}{1 + 2.8(f/f_{\text{col}})^{3.8}} \tag{3.15}$$

Finally, we can now write the complete numerically simulated GW energy density pa-

rameter as [28],

$$h^2\Omega_{\rm col}(f) = 1.67\times10^{-5}\left(\frac{100}{g^*}\right)^{1/3}\left(\frac{H_*}{\beta}\right)^2\kappa^2\left(\frac{0.11v_b^3}{v_b^2+0.42}\right)\left(\frac{\alpha}{1+\alpha}\right)^2 S_{\rm col}(f), \tag{3.16}$$

where κ is the fraction of the latent heat that is stored in an infinitely thin shell according to the envelope approximation.

Contribution from Sound Waves

We have previously discussed how sound waves are formed in the plasma as a result of the rapid expansion and merger of bubbles. It is expected that the bubble wall velocity v_b becomes constant after being initially accelerated. Hence, in this case we approximate the latent heat fraction $\kappa_{\rm sw}$ for non-runaway(bubbles which attain a relativistic terminal velocity) bubbles as [19],

$$\kappa_{\rm sw} \approx \begin{cases} \alpha(0.73+0.083\sqrt{\alpha}+\alpha)^{-1}, & v_b\sim 1 \\ \\ v_b^{6/5}6.9\alpha(1.36-0.037\sqrt{\alpha}+\alpha)^{-1}, & v_b\leq 0.1. \end{cases} \tag{3.17}$$

In the case of sound waves, the exact for of the peak frequency is not known with confidence. However, the estimated form of the peak frequency after redshift is given as [25],

$$f_{\rm sw} = \frac{1}{v_b}\left(\frac{T_*}{100GeV}\right)\left(\frac{H_*}{\beta}\right)^{-1}\left(\frac{g_*}{100}\right)^{1/6}\times 1.9\times10^{-5}{\rm Hz}. \tag{3.18}$$

Similar to the case of bubble collisions, we have $S_{\rm sw}$ as the numerically fitted spectral shape of the corresponding GW contribution and is given by,

$$S_{\rm sw}(f) = \left(\frac{7}{4+3(f/f_{\rm sw})}\right)^{7/2}(f/f_{\rm sw})^3. \tag{3.19}$$

Hence the gravitational energy density parameter formed by the sound waves is numerically simulated to be [25],

$$h^2\Omega_{\rm sw}(f) = 2.65\times10^{-6}\left(\frac{100}{g^*}\right)^{1/3}\left(\frac{H_*}{\beta}\right)\kappa^2\left(\frac{\alpha}{1+\alpha}\right)^2 v_b S_{\rm sw}(f). \tag{3.20}$$

The important aspect to consider here is that the spectral amplitude (3.20) in the case of sound waves is enhanced by a factor of $\frac{\beta}{H_*}$ as compared to that in case of bubble collisions (3.16). This is due to the fact that the sound waves generated from bubble collisions are present in the plasma, even after the bubble collisions are over and eventually die down slowly [11]. Hence the resultant gravitational waves generated from sound waves have a longer lifetime as compared to their bubble collision counterpart.

Contribution from MHD Turbulence

In our discussion on the GW energy density parameter arising from GWs, we begin with describing the form of the latent heat fraction in this case. Since both MHD turbulence and sound waves occur as a result of fluid motion, their latent heat fraction are related as,

$$\kappa_{\rm mhd} = \epsilon \kappa_{\rm sw} \tag{3.21}$$

Current simulations suggest that turbulence amounts to almost 5-10% [11] of the bulk motion of the fluid. We consider ϵ =0.05, even the exact number is yet unkown as it depends on the relation of MHD turbulence with sound waves.

Now, the redshifted peak frequency $f_{\rm mhd}$ is known to take the form [9],

$$f_{\rm mhd} = \frac{1}{v_b}\left(\frac{T_*}{100GeV}\right)\left(\frac{H_*}{\beta}\right)^{-1}\left(\frac{g_*}{100}\right)^{1/6} \times 2.7 \times 10^{-5}{\rm Hz}, \tag{3.22}$$

where as the spectral shape, $S_{\rm mhd}(f)$ is given as,

$$S_{\rm mhd}(f) = \frac{\left(f/f_{\rm mhd}\right)^3}{(1+8\pi f/h_*)\left[1+(f/f_{\rm mhd})\right]^{11/3}}. \tag{3.23}$$

Finally, the energy density parameter of the GW produced through turbulence in ionized plasma is estimated as [9],

$$h^2\Omega_{\rm mhd}(f) = 3.35 \times 10^{-4}\left(\frac{100}{g^*}\right)^{1/3}\left(\frac{H_*}{\beta}\right)\kappa^{3/2}\left(\frac{\alpha}{1+\alpha}\right)^{3/2} v_b S_{\rm mhd}(f). \tag{3.24}$$

Now these three contributions can be added linearly to form the total expected stochastic GW spectra. Hence the total GW energy density parameter is given as,

$$h^2\Omega_{\rm GW} = h^2\Omega_{\rm collisions} + h^2\Omega_{\text{sound waves}} + h^2\Omega_{\rm mhd}. \tag{3.25}$$

Given that we now know the exact form of the gravitational wave signal that we expect to detect, in the next section we briefly describe which BSM models could give rise to such GWs.

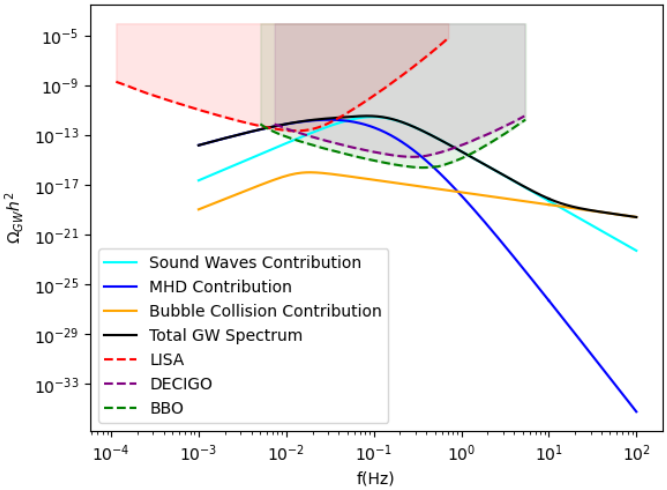

Fig. 3.1: GW spectra for a BSM theory with a new scalar, the total gravitational wave spectra expected to be observed plotted along with its component contributions by bubble collisions, MHD turbulence and sound waves.

4. SM EXTENSIONS WITH FIRST ORDER PHASE TRANSITIONS

4.1 Introduction

As the universe cools down, it attains a temperature at which the two vacua become degenerate in energy. This is called critical temperature (T_c) and it is proportional to the Higgs boson mass. It is also dependent to the gauge boson and top quark Yukawa couplings. However, extensions to the SM alter the Higgs mass as will be discussed in the subsequent section. This change in the mass of the Higgs boson in turn changes the T_c of the universe [1]. The standard model is known to have a crossover transition. So, if SM was complete theory, we would expect no primordial GWs to be observed by the upcoming GW detectors. But since it is now well established that the SM is not complete, we look for clear experimental signatures of BSM physics through GWs as many BSM theories are known to undergo a first order PT [23, 39, 21].

In our analysis, we consider different extensions of the SM and compute the corresponding gravitational spectra using the python package `CosmoTransitions` [43]. This package was primarily made for analysing finite temperature cosmological phase transitions driven by single or multiple scalar fields. We further adapt this package to analyse the vector boson and fermion extensions of the SM by making minor changes in the code. As a result, in the extended SM regime, now if the PT temperature (at which the bubbles can expand enough for a successful phase transition) is greater than the new T_c, a first order PT would be possible. A similar scenario can obtained by including new gauge or Yukawa coupling which can alter the T_c of the universe. We hence discuss such cases in this chapter.

4.2 Singlet Scalar extension

We start our analysis by considering the simplest possible model of with a real singlet scalar extension to the Higgs sector of the SM. This model holds special significance since it forms a part of many dark matter theories currently being considered. The lagrangian

of this extended Higgs sector becomes

$$\mathcal{L}_{\text{Higgs+Scalar}} = (D^\mu H)^\dagger (D_\mu H) + \frac{1}{2}(D^\mu S)^\dagger (D_\mu S) - V_{\text{eff}}(H, S), \tag{4.1}$$

where S is the scalar singlet (with vacuum expectation value v_s), D^μ is the covariant derivative ($D^\mu = \partial_\mu - i\frac{g'}{2}YB_\mu - i\frac{g}{2}\sigma_j W^j_\mu - i\frac{g_s}{2}\lambda_\alpha G^\alpha_\mu$, where g' is the coupling between the Y hypercharge and the B boson, g between the weak isospin σ_j and three vector bosons W^j and finally g_s is the coupling for the strong interaction and G is the gluon gauge field), $V_{\text{eff}}(H, S)$ is the potential of the H and S fields upto 1 loop corrections and H is the scalar Higgs doublet (with vacuum expectation value v=246.22 GeV) given by,

$$H = \frac{1}{\sqrt{2}} \begin{pmatrix} \chi_1 + i\chi_2 \\ v + h + i\chi_3. \end{pmatrix} \tag{4.2}$$

Also, we consider the tree level potential,

$$V_o(H, S) = -\mu_h^2 (H^\dagger H) + \lambda_h (H^\dagger H)^2 + \sigma (H^\dagger H) S + \tau (H^\dagger H)(S^2) + \frac{\mu_s^2}{2}(S^2) + \frac{\mu_3}{3} S (S^2) + \frac{\lambda_s}{4}(S^2)^2. \tag{4.3}$$

We now consider the following two minimization conditions by making (v, v_s) as the absolute minima of the fields (h, s). The conditions are:

$$\left.\frac{\partial V_o(H, S)}{\partial h}\right|_{v, v_s} = 0 \implies \mu_h^2 = \lambda_h v^2 + \sigma v_s + \tau v_s^2, \tag{4.4}$$

$$\left.\frac{\partial V_o(H, S)}{\partial S}\right|_{v, v_s} = 0 \implies \mu_s^2 = -\frac{1}{v_s}\left[\frac{v^2}{2}(\sigma + 2\tau v_s) + v_s^2(\mu_3 + \lambda_s v_s)\right], \tag{4.5}$$

where h is as defined in (4.2). To find the Goldstone boson mass, we replace (4.2) in (4.3) and identify the coefficient of χ^2 term as $\frac{1}{2}$ of the m_χ^2 to get,

$$m_\chi^2 = -\mu_h^2 + \lambda_h (h^2 - 2v^2) + \sigma S + \tau S^2. \tag{4.6}$$

To calculate the masses of h and S, we find the eigenvalues of the 2×2 Hessian matrix containing the partial derivatives of V_o w.r.t. h and S. The Hessian in general for a theory containing n scalar fields is given as:

$M^2_{h,s} = \begin{pmatrix} \frac{\partial^2 V_o}{\partial h^2} & \frac{\partial^2 V_o}{\partial h \partial s} \\ \frac{\partial^2 V_o}{\partial s \partial h} & \frac{\partial^2 V_o}{\partial s^2} \end{pmatrix}$

For the potential given in (4.3) for the scalar theory considered here,

$$M^2_{h,s} = \begin{pmatrix} -\mu_h^2 + \sigma S + 3\lambda_h h^2 + \tau S^2 & \sigma h + 2\tau h S \\ \sigma h + 2\tau h S & \tau h^2 + 3\lambda_s S^2 + 2\mu_3 S + \mu_s^2 \end{pmatrix}$$

The eigenvalues of M^2 are hence identified with the squared masses of h and S.

$$m^2_{h,s} = m^2_{1,2} = \frac{1}{2}[(3\lambda_s + \tau)S^2 + (3\lambda_h + \tau)h^2 + (\sigma + 2\mu_3)S - \mu_h^2 + \mu_s^2 \\ \mp \{((3\lambda_h - \tau)h^2 - (3\lambda_s - \tau)S^2 + (\sigma - 2\mu_3)S - \mu_h^2 - \mu_s^2)^2 + 4(2\tau S + \sigma)^2 h^2\}^{\frac{1}{2}}]. \quad (4.7)$$

Note that the Higgs mass and all the Goldstone boson masses have extra terms due to the presence of a new scalar field. However such terms are not seen in case of the the W, Z and top quark masses as they are determined by the Yukawa coupling which remains unaffected by the addition of this new scalar in the theory.

4.2.1 Free Parameters of the Theory

Based on the tree level potential given in (4.3), we start with 8 free parameters namely, $v_s, \lambda_s, \tau, \lambda_h, \mu_h, \sigma, \mu_3$ and μ_s. After imposing the conditions in (5.9) and (4.5) we are left with 6 free parameters. Now, in order to be consistent with experimental observations, we need to maintain the Higgs mass to the observed value of 125 GeV. This additional constraint can be incorporated by introducing the 'Higgs Mass parameter' $m_h = 125GeV$ as is done in [2] and comparing the field 'h' and m_h dependent Higgs Boson masses with the μ_h^2 and λ_h dependent masses derived from our calculation in (4.17). We hence find that:

$$\mu_h^2 = \frac{m_h^2}{2}, \qquad \lambda_h = \frac{m_h^2}{2v^2} \quad (4.8)$$

The relations above can be further used in (5.9) to get the following relation,

$$\tau = -\frac{\sigma}{v_s}. \quad (4.9)$$

Hence, by the imposing the Higgs Boson mass condition, we are left with 6 parameters $v_s, \lambda_s, m_h, \sigma, \mu_3$ and μ_s. Furthermore, to ensure that the potential is bounded from below, we need τ, λ_s and λ_h such that $\tau + 2\sqrt{\lambda_s \lambda_h}$, λ_s, λ_h are all positive. Now, in the perturbative regime, the parameter space is further restricted by the conditions, $0 < \lambda_s < \sqrt{4\pi}$ and $0 < \lambda_h < \sqrt{4\pi}$, the later of which is trivially satisfied from the experimentally known fixed values of m_h=125 GeV and v=246 GeV.

4.2.2 Computations using `Cosmotransitions`

We use the functions `calcTcTrans()` and `TnTrans()` to find the critical temperature and the bubble nucleation temperature (temperature at which the first bubble of the PT is formed) of the transition. It also gives us information on the pressure difference, energy difference and the value of action for the PT. We then calculate the GW parameters: α_{GW} (latent heat fraction of the bubble), β (nucleation rate), κ_{sw} (latent heat fraction of sound waves), $v_b(\alpha_{\text{GW}})$ (bubble wall velocity as a function of α_{GW}) from the formulas given in [25, 19, 30] as mentioned in Section 3.4 and 2.5.2.

4.2.3 Results

Multiple combinations of parameter values were tested to find the strongest GW. The following calculated parameter values were used for plotting the strongest possible GW spectra:

Parameters	v_s	μ_3	σ	λ_s
Values(GeV)	300	-8.7459	-0.157	0.1

Tab. 4.1: Input parameters for the SM+scalar case.

For the relations discussed before, the parameter λ_h has a value of 0.129. Based on these parameters, using `CosmoTransitions`, we calculate the GW spectra parameters.

Results	T_{critical}	$T_{\text{nucleation}}$	α_{GW}	κ_{sw}	β
Values	120.32K	34.08K	0.51	0.39	2.16 $\times 10^7$ Joules

Tab. 4.2: Output parameters for the SM+ scalar case.

4.3 Fermion extension

Taking inspiration from the fermion model described in [2], we consider a model with a new singlet fermion $\mathcal{N}'$ which couples with a new left handed leptonic doublet $L_L = \begin{pmatrix} \mathcal{N} \\ \mathcal{E} \end{pmatrix}$, where $\mathcal{N}$ is the new neutrino and electron analogues. The lagrangian is given as:

$$\mathcal{L}_{Higgs+Le_L+\mathcal{N}'} = (D^\mu H)^\dagger (D_\mu H) + y_{\mathcal{N}_R} \bar{L}_L \tilde{H} \mathcal{N}'_R + y_{\mathcal{N}_L} \bar{\mathcal{N}'}_L \tilde{H}^\dagger L_R + m_L \bar{L'}_L L'_R + m_{\mathcal{N}} \bar{\mathcal{N}'} \mathcal{N}' + h.c. \quad (4.10)$$

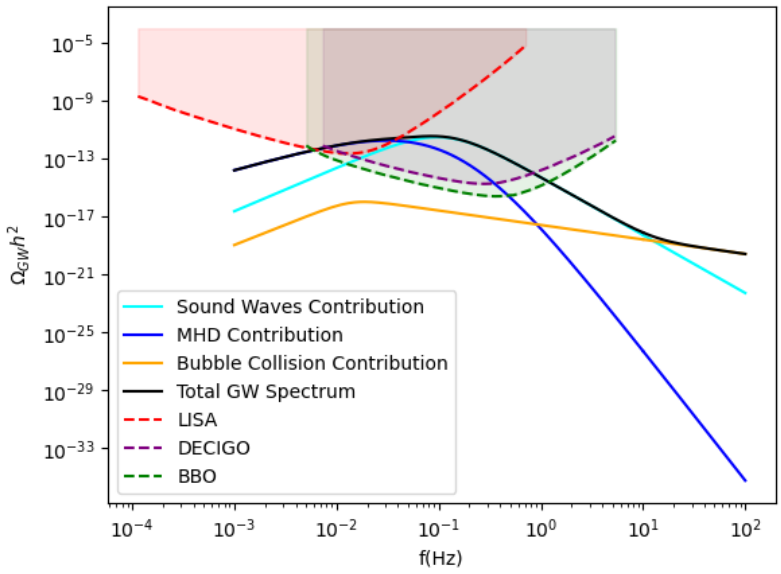

Fig. 4.1: Total Spectrum for the SM+Scalar case which peaks around 0.084Hz and so can be detected by LISA, DECIGO and BBO.

Here y_Z (where $Z = \{\mathcal{N}_L, \mathcal{N}_R\}$) correspond to the Yukawa coupling constants. $m_\mathcal{N}$ is the mass of the fermion $\mathcal{N}'$ and m_L is the mass of the fermion doublet L. We have $\tilde{H} = i\tau_2 H^*$, where H^* is the complex conjugate of the Higgs field, τ_2 is the 2nd Pauli matrix and $H^\dagger$ is the hermitian adjoint. H, $H^\dagger$and $\tilde{H}$ has hyper charges +1 , -1 and -1 respectively. L have hyper charge +1 analogous to the SM leptonic doublets. Hence the terms are chosen to make the Lagrangian $SU(2)$ invariant.
We then write the neutral and charged mass matrix as:

$$\mathcal{M}_\mathcal{N} = \begin{pmatrix} m_L & v y_{\mathcal{N}_L} \\ v y_{\mathcal{N}_R} & m_\mathcal{N} \end{pmatrix} \tag{4.11}$$

Each mass matrix can now be used to calculate the Higgs field (h) dependent fermion masses by diagonalizing $\mathcal{M}_X^\dagger \mathcal{M}_X$, where $X = \{\mathcal{N}\}$ in this case. We hence obtain the mass squared values (n^2) as,

$$n^2_{X_{1,2}}(h) = \frac{1}{2}\Bigg(m_L^2 + m_X^2 + \frac{y^2_{X_L} + y^2_{X_R}}{2}h^2 \mp \sqrt{\left(m_L^2 + m_X^2 + \frac{y^2_{X_L} + y^2_{X_R}}{2}h^2\right)^2 - (2m_L m_X - y_{X_L} y_{X_R} h^2)^2}\Bigg) \tag{4.12}$$

where X is as defined above.
The tree level potential is simply given by,

$$V_o(H) = -\mu^2(H^\dagger H) + \lambda(H^\dagger H)^2. \tag{4.13}$$

We now consider the following minimization condition by making (v) as the absolute minima. The condition is:

$$\left.\frac{\partial V_o(H)}{\partial h}\right|_v = 0 \implies \mu_h^2 = \lambda_h v^2. \tag{4.14}$$

$$\tag{4.15}$$

We find the Goldstone boson by repeating the same procedure as done for the scalar extension and get,

$$m_\chi^2 = -\mu_h^2 + \lambda_h h^2. \tag{4.16}$$

Using the Hessian formalism similar to the one used for the scalar extension, mass of the Higgs is computed to be

$$m_h^2 = -\mu_h^2 + 3\lambda_h h^2. \tag{4.17}$$

4.3.1 Free Parameters of the Theory

Based on the tree level potential given in (4.3), we start with 6 free parameters namely, $y_{\mathcal{N}_R}, y_{\mathcal{N}_L}, m_{\mathcal{N}}, m_L, \mu$ and λ. After imposing the condition in (4.14) we are left with 5 free parameters. Similar to the singlet scalar case, we now introduce the Higgs boson mass constraint using 'm_h' by following the same comparison as in [2], to get the relations (4.8) which also satisfy the condition (4.14). Hence, by the imposing the Higgs Boson mass condition, we are left with 4 parameters $y_{\mathcal{N}_R}, y_{\mathcal{N}_L}, m_{\mathcal{N}}$ and m_L. Furthermore, to ensure that the potential is bounded from below, we need λ such that it is always positive. Now, in the perturbative regime, the parameter space is further restricted by the condition, $0 < \lambda < \sqrt{4\pi}$ which is trivially satisfied from the experimentally known fixed values of m_h=125 GeV and v=246 GeV.

4.3.2 Results

Multiple combinations of parameter values were tested to find a first order phase transition. For the sake of simplicity, we consider $y_{\mathcal{N}_R}, y_{\mathcal{N}_L} = y$. Parameter scans were conducted in the following ranges: $2 < y < \sqrt{4\pi}$, $5 < m_{\mathcal{N}} < 1500$, $5 < m_L < 1500$.

Following is an example of the FOPT found for $\lambda = 0.1288$, as calculated in Section 4.3.1:

Based on these parameters, using `CosmoTransitions`, we calculate the GW spectra parameters.

Parameters	y	$m_{\mathcal{N}}$	m_L
Values(GeV)	2.10	124.50	78.96

Tab. 4.3: Input parameters for SM+ Fermion case.

Results	T_{critical}	T_{nuc}	α_{GW}	κ_{sw}	β
Values	43.28K	43.28K	0.0008	0.001	1.04×10^{11}Joules

Tab. 4.4: Output parameters for SM+ Fermion case.

4.4 Vector Boson Extension with a new scalar

We now consider a model that involves a new vector boson $\mathcal{V}$ with a corresponding U(1) gauge symmetry and scalar S that is essential for mass generation of the boson. As an analog to the SSB in the electroweak sector, the new scalar field breaks U(1) symmetry to form a new Goldstone boson which in turn generates mass for $\mathcal{V}$. After SSB , the scalar field mass dependent term for $\mathcal{V}$ is given as,

$$M_{\mathcal{V}} = \frac{m_v^2 S^2}{4}. \tag{4.18}$$

Here m_v is a new coupling parameter associated with $\mathcal{V}$. The lagrangian is similar to the single scalar extension case with the only difference now being that the SM covariant derivative D_μ is replaced by the new covariant derivative $\mathcal{D}_\mu = D_\mu + ig_{\mathcal{V}} T_a \mathcal{V}_\mu^a$, where T_a belongs to the set of generators of the U(1) group. The lagrangian is hence given as,

$$\mathcal{L}_{\text{Higgs+Scalar+VectorBoson}} = (\mathcal{D}^\mu H)^\dagger (\mathcal{D}_\mu H) + \frac{1}{2}(\mathcal{D}^\mu S)^\dagger (\mathcal{D}_\mu S) - V_{eff}(H, S). \tag{4.19}$$

The potential has the same form as the singlet scalar extension case and subsequently all the other derived relations are identical to the scalar case discussed above.

4.4.1 Free Parameters of the Theory

Based on the tree level potential given in (4.3), we start with 9 free parameters namely, $v_s, m_v, \lambda_s, \tau, \lambda_h, \mu_h, \sigma, \mu_3$ and μ_s. After imposing the condition in (5.9) we are left with 8 free parameters. Introducing the Higgs boson mass constraint using 'm_h' by following the same comparison similar to the singlet scalar case 4.2.1, we obtain the same relations in (4.8) which can be further used in (5.9) to get the relation in (4.9). Hence, by the imposing the Higgs Boson mass condition, we are effectively left with 6 parameters $v_s, m_v, \lambda_s, \sigma, \mu_3$ and μ_s. Furthermore, to ensure that the potential is bounded from below, we need τ, λ_s and λ_h such that $\tau + 2\sqrt{\lambda_s \lambda_h}, \lambda_s, \lambda_h$ are all positive. Now, in the perturbative

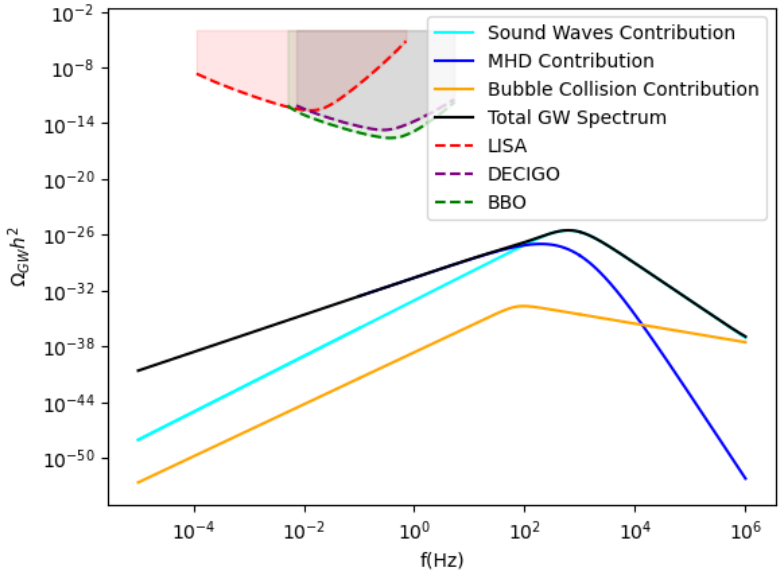

Fig. 4.2: Total Spectrum for the SM+Fermion case which peaks around 10^3 Hz and is very weak compared to the sensitivities of the GW detectors.

regime, the parameter space is further restricted by the conditions, $0 < \lambda_s < \sqrt{4\pi}$ and $0 < \lambda_h < \sqrt{4\pi}$, the later of which is trivially satisfied from the experimentally known fixed values of m_h=125 GeV and v=246 GeV.

4.4.2 Results

Multiple combinations of parameter values were tested to find the strongest GW. The following calculated parameter values were used for plotting the strongest possible GW spectra:

Parameters	vev_{scalar}	μ_3	σ	m_v (GeV)	λ_s
Values(GeV)	300	-8.76	-0.157	1.3	0.1

Tab. 4.5: Input parameters for SM+Scalar+Vector Boson case

For the relations discussed before, the parameter λ_h has a value of 0.129. Based on these parameters, using `CosmoTransitions`, we calculate the GW spectra parameters.

Results	T_{critical}	$T_{\text{nucleation}}$	α_{GW}	κ_{sw}	β
Values	119.57K	35.11K	0.46	0.37	2.37 $\times 10^7$ Joules

Tab. 4.6: Output parameters for SM+Scalar+Vector Boson case.

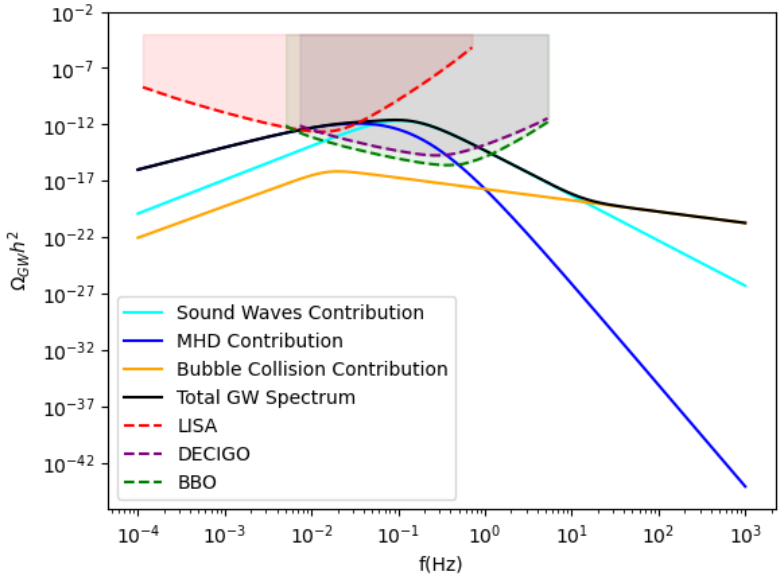

Fig. 4.3: Total Spectrum for the SM+Scalar+Vector case which peaks at 0.092 Hz and so can be detected by LISA, DECIGO and BBO.

It can hence be inferred that adding a vector boson does not significantly affect the phase transition as compared to that seen in case SM+ real Scalar in Section 4.2.

4.5 Analysis and Conclusions

In conclusion, this chapter discussed the preliminary analysis of standard model extensions of adding new particles individually to SM. To study the general effect of adding new particles, we include all possible interactions without any physical constraints. We see that while the SM + Scalar and SM + Scalar + Vector Boson cases give rise to a detectable GW, the SM + Fermion case produces a very weak GW, which cannot be detected. Furthermore, it is seen comparing with the real scalar case that, adding a vector boson restricts the FOPT parameter space above -8 (below 8 in magnitude), hence effectively reducing the strength of the phase transition in the specific parameter set. Thus, even though this chapter does not specifically study models addressing drawbacks of SM, it builds a foundation for studying physical BSM cases as will be discussed in the next chapter.

5. GRAVITATIONAL WAVES ARISING FROM DARK MATTER MODELS

5.1 Introduction

While the idea of 'Dark matter' (DM) was proposed as early as in the late 19th century, it eludes our complete understanding even today. It is proposed to be a type of matter which does not interact via the electromagnetic force, not emitting or absorbing electromagnetic radiation (light) which is why it is called dark. It is only known to interact with the visible (baryonic) matter through gravitational interaction which makes it challenging to detect. Perhaps the most striking signal of the presence of dark matter comes from the unexpected rotational velocities of stars in spiral galaxies. Spiral galaxies have a dense core full of stars and this density of stars fades as we move away from the core towards the disc edge. However, it is seen that the rotational velocity of stars in spirals becomes constant as we move outwards from the core, contrary to the expectation that rotational velocities should have a decreasing trend away from the core following the visible mass density trend [3]. This suggests the presence of a large scale non-visible mass distribution we call 'Dark Matter', which can hence be accounted for the rotational velocity being constant.

Even though multiple large scale evidences of the presence dark matter can be seen at astronomical scales, the specific properties of DM are highly model dependent [3]. Till date, many DM candidates like Weakly Interacting Massive Particles (WIMPs), axions, sterile neutrinos, etc. have been proposed. However they lack experimental verification. Even though dark matter makes around 27% of the total content of the universe, any DM direct detection efforts at high precision earth based experiments like XENON series (Noble gas Scintillators), CRESST (Cryogenic crystal detectors), etc. have not yet been successful in providing any conclusive evidence. In this final chapter, we propose a new technique that has the potential to experimentally verify the actual dark matter model based on the observed primordial GW spectra to be detected by upcoming space based GW detectors.

DM models

Perhaps the most widely accepted models describing the dark sector is the ΛCDM model which consists of a cosmological constant Λ (accounting for dark energy) and cold dark matter (CDM). However, this model fails to describe the precise nature of dark matter, thus posing an equally important question for CDM. With the aim to find observational insights into this decades long debate on the nature of DM, we primarily investigate 3 minimal dark matter models each with different types of DM particles in this study.

5.2 Scalar Dark Matter

Quite recently, many studies [14, 8, 24, 20] have theoretically suggested the possibility for DM to be of the scalar nature. For example, a study given in [12] describes the dark sector originating from a single scalar field with a pressureless component forming dark matter and a homogeneous component identified as dark energy. Thus, scalar BSM physics puts forth an interesting case for dark matter and hence is studied in this section.

5.2.1 Theory

To consider the simplest possible general case of DM, consider a SU(2) singlet, electrically neutral complex scalar field S describing dark matter. Similar to the discussion in Section 4.2, we have the potential,

$$V_o(H,S) = -\mu_h^2(H^\dagger H) + \lambda_h(H^\dagger H)^2 + \sigma(H^\dagger H)S + \tau(H^\dagger H)(S^\dagger S) + \frac{\mu_s^2}{2}(S^\dagger S) + \frac{\mu_3}{3}S(S^\dagger S) + \frac{\lambda_s}{4}(S^\dagger S)^2. \quad (5.1)$$

In order to describe a physical dark matter field, we need to ensure it's stability based on the interaction terms in 5.1, specifically $\sigma(H^\dagger H)S$ and $\tau(H^\dagger H)(S^\dagger S)$.

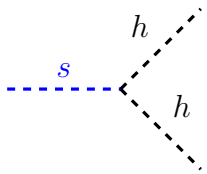

Fig. 5.1: The Feynman diagram representing the interaction from the term $\sigma(h)^2(s)$ which causes DM to decay into two Higgs particles.

The interaction from the tree level term $\sigma(H^\dagger H)S = \sigma(v_h + h)^2(v_s + s)$, where h and s are the Higgs and DM field components while v_h and v_s are the vacuum expectation values of the two fields respectively. Particularly the term $\sigma(h)^2(s)$ causes DM to decay

into two Higgs particles as represented in the diagram above.

Hence to ensure stability of the DM field, the term $\sigma(H^\dagger H)S$ is forbidden from the tree level potential. This can further be justified by imposing a global Z_2 symmetry, such that the scalar S transforms as -1 (i.e. S $\rightarrow$ -S) under the symmetry transformation. In such a case, the cubic term in S in the potential (5.1) naturally drops out as it does not remain invariant under such a Z_2 symmetry transformation.

However, in this case, we do not impose any such symmetry condition and hence the cubic term in S is allowed.

From $\tau(H^\dagger H)(S^\dagger S)$ we get the following interaction terms:

$$\tau(H^\dagger H)(S^\dagger S) = \tau(v_h + h)^2(v_s + s)^2 \tag{5.2}$$

$$= \tau h^2 s^2 + \tau v_h^2 s^2 + \tau h^2 v_s^2 + 4\tau v_h v_s hs + 2\tau v_h h s^2 + 2\tau v_s s h^2 + \text{const} \tag{5.3}$$

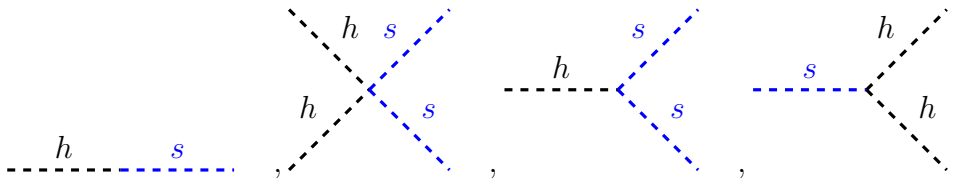

Fig. 5.2: The Feynman diagrams representing the interaction from the tree level term $\tau(v_h + h)^2(v_s + s)^2$; left to right: (1) $4\tau v_s v_h sh$: 2-point h-s scattering term, (2) $\tau s^2 h^2$: 4-point h-s scattering term, (3) $\tau s^2 v_h h$: Higgs decay into two DM particles, (4) $\tau h^2 v_s s$: DM decay into two Higgs particles.

Hence to ensure stability of the DM field, the term $\tau(h)^2 v_s s$ should be forbidden, however since $\tau(v_h + h)^2(v_s + s)^2$ represents a Higgs decay, and not a DM field decay it is allowed along with all other terms in 5.3. Thus in order to remove $\tau h^2 v_s s$, we take a DM field with $v_s = 0$.

The rest of the computations remain the same as derived in Section 4.2 for the scalar singlet case.

5.2.2 Results

Multiple combinations of parameter values were tested to find the strongest GW. The following calculated parameter values were used for plotting the strongest possible GW spectra:

Parameters	vev_{scalar}	τ	μ_3	σ	λ_s
Values(GeV)	0.000001	0.1488254	–3.56	0.0	0.225399

Tab. 5.1: Input parameters for SM + Scalar DM case.

For the relations discussed before, the parameter λ_h has a value of 0.129. Since we consider a complex scalar DM model, the degree of freedom is 2 for the field. Based on these parameters, using `CosmoTransitions`, we calculate the GW spectra parameters.

Results	T_{critical}	$T_{\text{nucleation}}$	α_{GW}	κ_{sw}	β
Values	116.24K	64.12K	0.10	0.117	1.68×10^8 Joules

Tab. 5.2: Output parameters for SM + Scalar DM case.

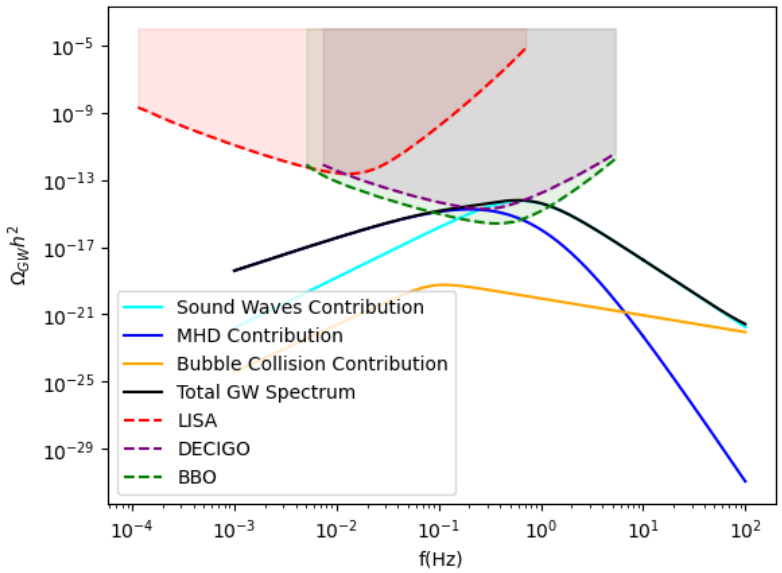

Fig. 5.3: Total Spectrum for the SM+ DM Scalar case which peaks around 0.596 Hz and so can be detected by DECIGO and BBO.

5.3 Fermionic Dark Matter

Since the most prominent effects of dark matter have been observed in astrophysical scales, it is important to consider DM models that are developed in the context of astrophysics and cosmology. The exact nature of DM plays a crucial role in dictating the outcomes of non-linear structure formation processes like self-gravitating DM Halos [4]. Studies like the Ruffini-Argüelles-Rueda (RAR) Model [4], DM in spherical dwarf galaxies [41] and DM in stars [38] discuss galactic DM using a fermionic DM particle. Hence to

provide a robust experimental verification method for such models, we now extend our analysis to look at gravitational wave imprints of fermionic dark matter.

5.3.1 Theory

We consider a electrically neutral, SU(2) singlet fermion $\mathcal{N}$ as the DM particle. Based on the discussions in [6] and our results from Section 4.3, we also add a new, electrically neutral complex scalar S to the theory, such that we have the Yukawa term for the fermion is now $Y\bar{\mathcal{N}}S\mathcal{N}$, where Y is the Yukawa coupling constant. Thus the important terms of the Lagrangian are:

$$\mathcal{L}_{Higgs+\mathcal{N}} \supset Y\bar{\mathcal{N}}S\mathcal{N} + m_{\mathcal{N}}\bar{\mathcal{N}}\mathcal{N} + h.c. \tag{5.4}$$

In this model, we impose a global U(1) symmetry, with S having charge 0 while the DM fermion $\mathcal{N}$ has charge 1. which forbids any coupling terms between SM singlet fermions and the $\mathcal{N}$. This can physically be understood as a possible way to account for the negligible interaction that DM has with ordinary matter. The potential remains the same as that in (5.1). Hence the following diagram is possible.

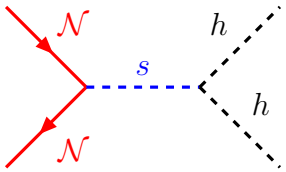

Fig. 5.4: The Feynman diagram representing the combined interaction from (a) the tree level term $\sigma(H^\dagger H)S = \sigma(v_h+h)^2(v_s+s)$ (where h and s are the Higgs and DM field components) and (b) the Yukawa term $Y\bar{\mathcal{N}}\mathcal{N}S$. We see that unlike the SM+ scalar case, the term $\sigma(h)^2(s)$ does not form an unstable DM, instead acts as a mediator in the DM - Higgs scattering diagram above.

5.3.2 Results

Multiple combinations of parameter values were tested to find the strongest GW. The following calculated parameter values were used for plotting the strongest possible GW spectra:

Parameters	vev_{scalar}	$m_{\mathcal{N}}$(GeV)	μ_3	σ	λ_s	Y
Values(GeV)	300	10	-0.716	-0.10	0.76	2.6

Tab. 5.3: Input parameters for SM + Scalar + Fermionic DM case.

For the relations discussed before, the parameter λ_h has a value of 0.129. Since we consider a complex scalar in the model, the degree of freedom is 2 for the field, while for the DM fermion, it is 4(from the Dirac representation). Based on these parameters, using `CosmoTransitions`, we calculate the GW spectra parameters.

Results	T_{critical}	$T_{\text{nucleation}}$	α_{GW}	κ_{sw}	β
Values	104.6809K	104.6804K	0.0007	0.0009	5.09×10^{13} Joules

Tab. 5.4: Output parameters for SM + Scalar + Fermionic DM case.

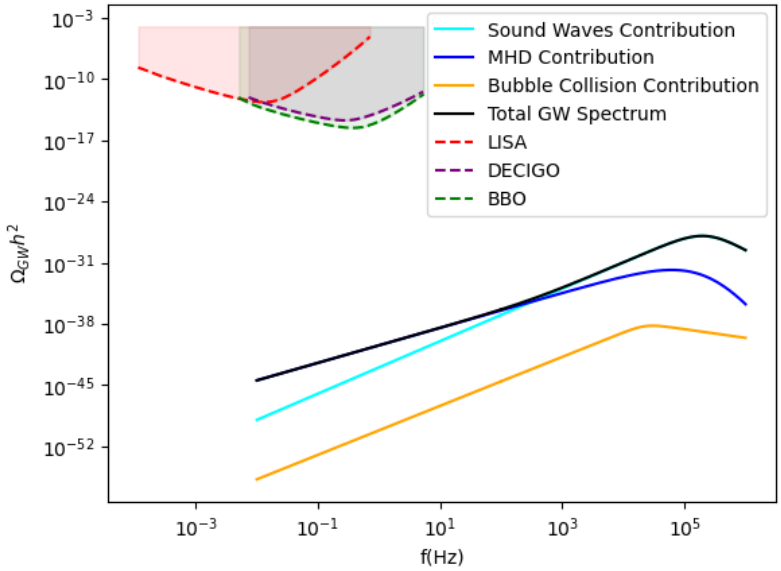

Fig. 5.5: Total Spectrum for the SM+ DM Fermion + Scalar case which peaks at 10^5 Hz and so cannot be detected by LISA, DECIGO or BBO.

Comparison with SM+Scalar Case

To study the effect of the fermion dark matter particle in our theory, we look at gravitational waves arising form a model without the fermionic DM particle. Hence we consider the potential (5.1). Now since the complex scalar is not a DM particle, no stability conditions are imposed and so all terms in the potential (5.1) are considered. Following is the GW spectra obtained keeping the SM+Scalar model parameters same as in the SM+Fermion+Scalar model above. Following are the parameters used:

Parameters	vev_{scalar}	μ_3	σ	λ_s
Values(GeV)	300	-8.76	-0.157	0.1

Tab. 5.5: Input parameters for SM + Complex Scalar case.

We find the following FOPT:

Results	T_{critical}	$T_{\text{nucleation}}$	α_{GW}	κ_{sw}	β
Values	119.5K	35.11K	0.46	0.37	2.37 $\times 10^7$ Joules

Tab. 5.6: Output parameters for SM + Complex Scalar case.

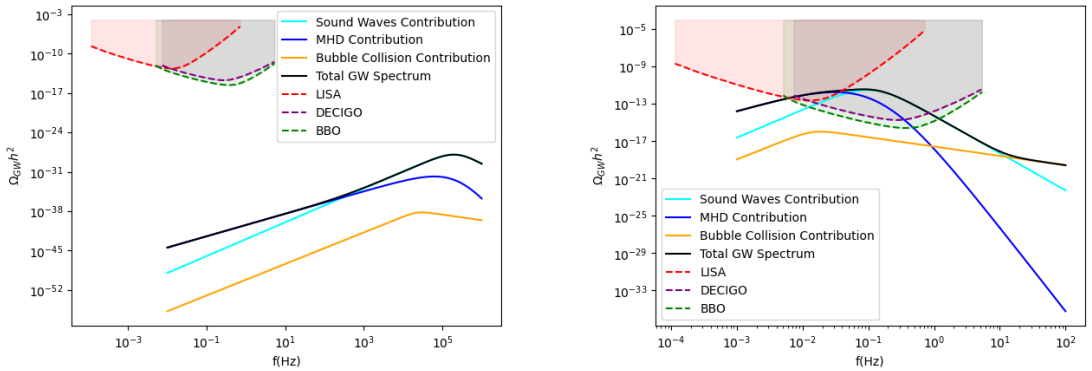

(a) SM+Scalar+Fermion **(b)** SM+Scalar

Fig. 5.6: Total Spectrum for the SM+ DM Fermion + Scalar case (Peak at 10^5 Hz) and the SM+ Complex Scalar case (Peak at 0.084 Hz) compared to the sensitivities of upcoming GW detectors.

Analysis

Multiple such parameter sets were tested to analyse the effect of an additional fermion particle to the SM+ Complex Scalar model. In each case, it is seen that adding a fermion greatly diminishes the strength of the resultant FOPT as can be seen in Figure 5.6. The nature of this result is in line with the weak GW spectra seen for the case of SM+ Fermion in Chapter 4.

5.4 Scalar DM with U(1) Gauge Extension

In this section, we consider a SM+ scalar DM (S_{DM}) model along with an additional complex scalar (S) which gives mass to a new neutral gauge boson (Z'). Furthermore, the $H, S_{DM}$and S fields hold a U(1) gauge symmetry each having a U(1) charge of 0,1 and 2. Hence cubic terms in all these fields (like $H^\dagger H)S$, $(S^\dagger S)S$, etc.) are forbidden from the potential in order to conserve this symmetry. The new gauge boson gets its mass from the scalar S by breaking a U(1) symmetry and the mass term can hence be written as :

$$M_{Z'} = \frac{1}{4} m_{Z'}^2 S^2, \tag{5.5}$$

where as the potential is given as,

$$V_o(H,S,S_{DM}) = -\mu_h^2 H^\dagger H + \lambda_h (H^\dagger H)^2 + \mu_{HS} H^\dagger H S^\dagger S - \frac{\mu_s^2}{2} S^\dagger S + \frac{\lambda_s}{4}(S^\dagger S)^2 + \frac{\mu_D^2}{2} S_{DM}^\dagger S_{DM} + \mu_{HD} H^\dagger H S_{DM}^\dagger S_{DM} + \mu_{SD} S^\dagger S S_{DM}^\dagger S_{DM} + \frac{\lambda_D}{4}(S_{DM}^\dagger S_{DM})^2. \quad (5.6)$$

We now substitute the following form for the Higgs field with the neutral goldstone boson explicitly given (to indicate that this is neutral imaginary degree of freedom G^o of the Higgs that gives mass to the neutral gauge boson Z').

$$H = \frac{1}{\sqrt{2}} \begin{pmatrix} 0 \\ v_\phi + \phi_R + i G^o \end{pmatrix}, \quad (5.7)$$

while the other two fields are,

$$S = (v_\sigma + \sigma_R + i\sigma_I), S_{DM} = (0 + \chi_R + i\chi_I) \quad (5.8)$$

It is worthwhile to note that in the above definitions, we explicitly show the vev of the fields to make it clear to the reader that the dark matter field S_{DM} has no vev. Now, substituting the above relations (5.7), (5.8) into the potential (5.6), we now consider the following three minimization conditions by making $(v, v_s, 0)$ as the absolute minima of the fields $(\phi_R, \sigma_R, \chi_R)$ where as the imaginary fields have 0 vevs. The conditions for the real field derivatives are:

$$\left.\frac{\partial V_o(\phi_R, G^o, \sigma_R, \sigma_I, \chi_R, \chi_I)}{\partial \phi_R}\right|_{v,v_s,0} = 0 \implies \mu_h^2 = \left[\lambda_h v_\phi^2 + \mu_{HS} v_\sigma^2\right], \quad (5.9)$$

$$\left.\frac{\partial V_o(\phi_R, G^o, \sigma_R, \sigma_I, \chi_R, \chi_I)}{\partial \sigma_R}\right|_{v,v_s,0} = 0 \implies \mu_S^2 = \left[\lambda_h v_\sigma^2 + \mu_{HS} v_\phi^2\right], \quad (5.10)$$

$$\left.\frac{\partial V_o(\phi_R, G^o, \sigma_R, \sigma_I, \chi_R, \chi_I)}{\partial \chi_R}\right|_{v,v_s,0} = 0 \implies \mu_D^2 = -(\mu_{HD} v_\phi^2 + 2\mu_{SD} v_\sigma^2), \quad (5.11)$$

We now split the problem into two parts: The real and imaginary fields. For the real fields $(\phi_R, \sigma_R, \chi_R)$, the Hessian matrix is hence given as,

$$M^2_{\text{Real}} = \begin{pmatrix} \frac{\partial^2 V_o}{\partial \phi_R^2} & \frac{\partial^2 V_o}{\partial \phi_R \partial \sigma_R} & \frac{\partial^2 V_o}{\partial \phi_R \partial \chi_R} \\ \frac{\partial^2 V_o}{\partial \sigma_R \partial \phi_R} & \frac{\partial^2 V_o}{\partial \sigma_R^2} & \frac{\partial^2 V_o}{\partial \sigma_R \partial \chi_R} \\ \frac{\partial^2 V_o}{\partial \chi_R \partial \phi_R} & \frac{\partial^2 V_o}{\partial \phi_R \partial \sigma_R} & \frac{\partial^2 V_o}{\partial \chi_R^2} \end{pmatrix}$$

Now the Hessian matrix for the potential given in (5.6) in the DM model considered

here is,

$$M^2_{\text{Real}} = \begin{pmatrix} 2\lambda_h v_\phi^2 & 2\mu_{HS} v_\phi v_\sigma & 0 \\ 2\mu_{HS} v_\phi v_\sigma & 2\lambda_s v_\sigma^2 & 0 \\ 0 & 0 & 2\lambda_D \chi_R^2. \end{pmatrix}$$

Since the dark matter field has a 0 vev following stability conditions similar to those discussed in Section 5.2, $2\lambda_D \chi_R^2 = 0$ The eigenvalues of M^2 are hence identified with the squared masses of ϕ_R, σ_R and χ_R.

$$m_(\phi_R)^2 = \lambda_h v_\phi^2 + \mu_{HS} v_\phi v_\sigma - \sqrt{\lambda_h^2 v_\phi^4 + 4 v_\sigma^4 \lambda_s^2 - 2\lambda_h v_\phi^3 \mu_{HS} v_\sigma + \mu_{HS}^2 v_\phi^2 v_\sigma^2}, \tag{5.12}$$

$$m_(\sigma_R)^2 = \lambda_h v_\phi^2 + \mu_{HS} v_\phi v_\sigma + \sqrt{\lambda_h^2 v_\phi^4 + 4 v_\sigma^4 \lambda_s^2 - 2\lambda_h v_\phi^3 \mu_{HS} v_\sigma + \mu_{HS}^2 v_\phi^2 v_\sigma^2}, \tag{5.13}$$

$$m_(\chi_R)^2 = 0. \tag{5.14}$$

We now perform a similar analysis for the imaginary fields (G^o, σ_I, χ_I) and get the following Hessian matrix,

$$M^2_{\text{Img}} = \begin{pmatrix} 2\lambda_h (G^o)^2 & 2\mu_{HS} G^o \sigma_I & 0 \\ 2\mu_{HS} G \sigma_I & 2\lambda_s \sigma_I^2 & 0 \\ 0 & 0 & 2\lambda_D \chi_I^2 \end{pmatrix}$$

Since all the imaginary fields have a 0 vacuum expectation value, the all Hessian matrix terms become 0, thus indicating 0 tree level masses for all three fields G^o, σ_I and χ_I.

Hence the tree level masses (5.12), (5.13), (5.14) found for the the real fields as well as the 0 masses for imaginary fields are then inserted into `Cosmotransitions` along with their degrees of freedom taken as 1 to compute the GW spectra. Even after testing multiple parameter sets, we do not find a FOPT in this model.

5.5 Fermionic DM with U(1) Gauge Extension

Now consider a fermionic DM model similar to the one discussed in Section 5.3 while adding a new gauge boson $\mathcal{V}$ and a new complex scalar S. We impose a U(1) symmetry on the fermion, which forbids certain coupling terms with other SM fields, that have an odd number of fermions coupling together. The new gauge boson gets its mass from the scalar by breaking a U(1) symmetry and the mass term can hence be written as :

$$M_{\mathcal{V}} = \frac{1}{4} m_v^2 S^2. \tag{5.15}$$

Based on the discussions in Figure 5.4, we include S cubic terms as well in our potential (which is the same as (5.1)).

In order to make a direct comparison with the earlier cases, we keep the common parameters same as before, while testing different values for the new parameters to find the strongest GW spectra. We find the following strongest possible GW spectra with the following parameters:

Parameters	vev_{scalar}	$m_{\mathcal{N}}$	μ_3	σ	λ_s	Y	$m_{\mathcal{V}}$
Values(GeV)	300	4.2	-6.29	-0.31	0.64	2.5	1.3

Tab. 5.7: Input parameters for SM + Scalar + Fermionic DM + Vector Boson case.

For the relations discussed before, the parameter λ_h has a value of 0.129. Since we consider a complex scalar in the model, the degree of freedom is 2 for the field, while for the DM fermion, it is 4 (from the Dirac representation). The degrees of freedom for the new gauge boson are 3. Based on these parameters, using `CosmoTransitions`, we calculate the GW spectra parameters.

Results	T_{critical}	$T_{\text{nucleation}}$	α_{GW}	κ_{sw}	β
Values	109.8273K	109.8268K	0.00018	0.00024	9.78 $\times 10^{11}$ Joules

Tab. 5.8: Output parameters for SM + Scalar + Fermionic DM + Vector Boson case.

5.6 Analysis

The final chapter sheds light on the differences in cosmological phase transitions that occurred in the 4 dark matter models in the form of their GW spectra. It is seen that while the scalar DM model produces an observable GW spectra, the same in not seen in cases of SM + scalar + fermionic dark matter and SM + scalar + fermionic dark matter with a U(1) gauge extension. Even though a first order phase transition occurs in all three cases, the strength of the PT varies considerably for the fermionic DM case making it undetectable within current limits even after adding a gauge boson to the model. In fact, comparing the results from the last two cases, it is seen that adding a gauge boson, makes the phase transition weaker. However, for the case of a SM + Scalar + Scalar DM, we could not find a first order PT. Hence we conclude that GWs can not only distinguish between SM and SM extensions, but can also provide us with crucial information about the constituents of the BSM theory.

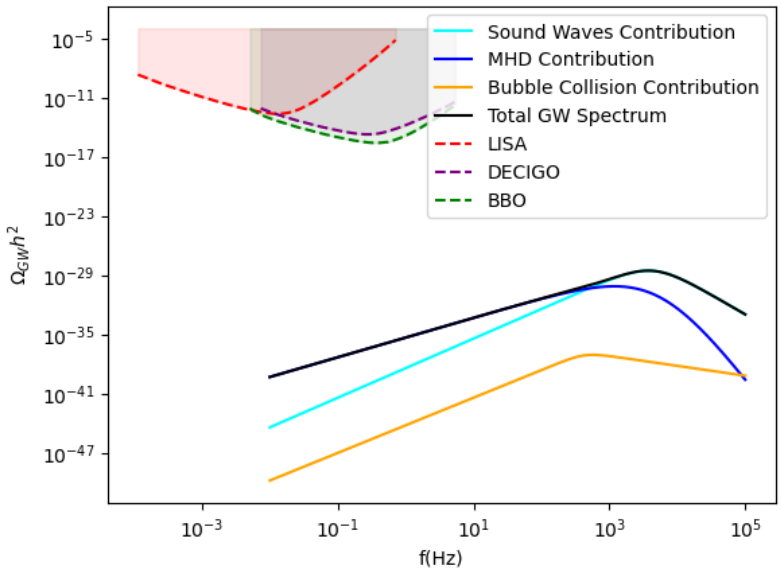

Fig. 5.7: Total Spectrum for the SM+ DM Fermion + Scalar + Vector case which peaks at 3.7×10^3 Hz and is very weak compared to the sensitivities of the GW detectors.

6. CONCLUSIONS

This thesis is aimed at studying the cosmological effect of different possible standard model extensions, specifically detectable through upcoming GW detectors like LISA, DECIGO and BBO. We analyse the most fundamental scalar extension of SM to understand its effect on the resulting PT of the universe. It is seen that the additional scalar changes the effective finite temperature potential of the universe, thus causing a first order phase transition (FOPT) which would otherwise have been a second order phase transition (SOPT) for SM.

Subsequently, we extend our analysis to the fermion and vector boson extensions of the standard model and compute the possible GW arising from them. While the cases of a real new scalar and a new gauge boson give rise to a strong FOPT, we find that the fermion extension undergoes a weak FOPT(not currently detectable) given that the Higgs mass is kept constant to the experimentally observed value of 125 GeV. However, the SM + Scalar and SM + Gauge Boson models are seen to produce detectable GWs through strong FOPTs. From these generalized SM extensions, we conclude that GWs act as an efficient probe in distinguishing between SM and SM + new particle cases.

Using the above three scenarios as a preliminary analysis, we now study the GW spectra arising from dark matter models. Specifically we study the BSM cases that include a scalar DM field, a fermion DM + new scalar, a new scalar + scalar DM with U(1) gauge extension and a fermion DM + new scalar with U(1) gauge extension imposing DM stability conditions. We find the strongest FOPT in the case of SM + Scalar DM which falls well within the detectable ranges of DECIGO and BBO. A similar case is seen for the SM + Fermionic DM + Scalar , but the FOPT is weaker than the Scalar DM model and hence the GW cannot be detected. It is also observed that the presence of a DM fermion significantly diminishes the FOPT and hence the GW spectra, as compared to the case of a simple SM + Complex Scalar extension model with the same parameters. Interestingly, though it was seen in Chapter 4 that adding a gauge boson slightly strengthened the FOPT for the SM + Scalar case, in Chapter 5 we see that this gauge extension leads to a weaker FOPT in case of SM + Fermionic DM + scalar model. This

might hint towards interesting fermion- gauge boson dynamics in the theory. In case of SM + scalar + Scalar DM, however, we do not find a FOPT.

Considering the different output parameters that govern the strength of the GW spectra, it is seen that a higher α and a lower β give rise to a stronger FOPT and hence a stronger GW spectra, however this analysis is tested to be true when compared within a single model. We compute the GW spectra to be within the frequency range of 10^{-2} Hz to 10^{5} Hz much of which overlaps with the current detectability range of 10^{-4} Hz to 10 Hz. Furthermore, we observe significant changes in the spectra, not only based on the presence of new particles but also the type of new particles in BSM theories. We hence confirm the validity of the technique of probing into new physics through stochastic GW observations.

BIBLIOGRAPHY

[1] Greg W Anderson and Lawrence J Hall. "Electroweak phase transition and baryogenesis". In: *Physical Review D* 45.8 (1992), p. 2685.

[2] Andrei Angelescu and Peisi Huang. "Multistep strongly first order phase transitions from new fermions at the TeV scale". In: *Physical Review D* 99.5 (2019), p. 055023.

[3] Alexandre Arbey and Farvah Mahmoudi. "Dark matter and the early Universe: a review". In: *Progress in Particle and Nuclear Physics* 119 (2021), p. 103865.

[4] Carlos Raúl Argüelles et al. "Fermionic dark matter: physics, astrophysics, and cosmology". In: *Universe* 9.4 (2023), p. 197.

[5] Daniel Baumann. "Cosmology, part iii mathematical tripos". In: *University lecture notes* 56 (2014), p. 34.

[6] C Boehm and Pierre Fayet. "Scalar dark matter candidates". In: *Nuclear Physics B* 683.1-2 (2004), pp. 219–263.

[7] Moritz Breitbach. "Gravitational Waves from Cosmological Phase Transitions". In: *arXiv preprint arXiv:2204.09661* (2022).

[8] Matthew R Buckley, David Feld, and Dorival Goncalves. "Scalar simplified models for dark matter". In: *Physical Review D* 91.1 (2015), p. 015017.

[9] Chiara Caprini, Ruth Durrer, and Geraldine Servant. "The stochastic gravitational wave background from turbulence and magnetic fields generated by a first-order phase transition". In: *Journal of Cosmology and Astroparticle Physics* 2009.12 (2009), p. 024.

[10] Chiara Caprini et al. "Detecting gravitational waves from cosmological phase transitions with LISA: an update". In: *Journal of Cosmology and Astroparticle Physics* 2020.03 (2020), p. 024.

[11] Chiara Caprini et al. "Science with the space-based interferometer eLISA. II: Gravitational waves from cosmological phase transitions". In: *Journal of cosmology and astroparticle physics* 2016.04 (2016), p. 001.

[12] Saulo Carneiro. "Can the cosmological dark sector be modeled by a single scalar field?" In: *General Relativity and Gravitation* 50.9 (2018), p. 114.

[13] Jens Chluba. "Tests of the CMB temperature–redshift relation, CMB spectral distortions and why adiabatic photon production is hard". In: *Monthly Notices of the Royal Astronomical Society* 443.3 (2014), pp. 1881–1888.

[14] James M Cline et al. "Update on scalar singlet dark matter". In: *Physical Review D* 88.5 (2013), p. 055025.

[15] Sidney Coleman and Erick Weinberg. "Radiative corrections as the origin of spontaneous symmetry breaking". In: *Physical Review D* 7.6 (1973), p. 1888.

[16] Vincent Corbin and Neil J Cornish. "Detecting the cosmic gravitational wave background with the big bang observer". In: *Classical and Quantum Gravity* 23.7 (2006), p. 2435.

[17] Karsten Danzmann, LISA Science Team, et al. "LISA—an ESA cornerstone mission for the detection and observation of gravitational waves". In: *Advances in Space Research* 32.7 (2003), pp. 1233–1242.

[18] Valentina De Romeri et al. "XENONnT and LUX-ZEPLIN constraints on DSNB-boosted dark matter". In: *arXiv preprint arXiv:2309.04117* (2023).

[19] Jose R Espinosa et al. "Energy budget of cosmological first-order phase transitions". In: *Journal of Cosmology and Astroparticle Physics* 2010.06 (2010), p. 028.

[20] Michele Frigerio et al. "Composite scalar dark matter". In: *Journal of High Energy Physics* 2012.7 (2012), pp. 1–36.

[21] Martin Gabelmann, M Margarete Mühlleitner, and Jonas Müller. "Electroweak phase transitions with BSM fermions". In: *Journal of High Energy Physics* 2022.1 (2022), pp. 1–16.

[22] Christophe Grojean and Geraldine Servant. "Gravitational waves from phase transitions at the electroweak scale and beyond". In: *Physical Review D* 75.4 (2007), p. 043507.

[23] Eleanor Hall et al. "Baryogenesis from a dark first-order phase transition". In: *Journal of High Energy Physics* 2020.4 (2020), pp. 1–15.

[24] Xiao-Gang He et al. "Constraints on scalar dark matter from direct experimental searches". In: *Physical Review D* 79.2 (2009), p. 023521.

[25] Mark Hindmarsh et al. "Numerical simulations of acoustically generated gravitational waves at a first order phase transition". In: *Physical Review D* 92.12 (2015), p. 123009.

[26] Mark Hindmarsh et al. "Phase transitions in the early universe". In: *SciPost physics lecture notes* (2021), p. 024.

[27] Mark Hindmarsh et al. “Shape of the acoustic gravitational wave power spectrum from a first order phase transition”. In: *Physical Review D* 96.10 (2017), p. 103520.

[28] Stephan J Huber and Thomas Konstandin. “Gravitational wave production by collisions: more bubbles”. In: *Journal of Cosmology and Astroparticle Physics* 2008.09 (2008), p. 022.

[29] Tina Kahniashvili, Leonard Kisslinger, and Trevor Stevens. “Gravitational radiation generated by cosmological phase transition magnetic fields”. In: *Physical review D* 81.2 (2010), p. 023004.

[30] Marc Kamionkowski, Arthur Kosowsky, and Michael S Turner. “Gravitational radiation from first-order phase transitions”. In: *Physical Review D* 49.6 (1994), p. 2837.

[31] Seiji Kawamura. “Primordial gravitational wave and DECIGO”. In: *Quest for the Origin of Particles and the Universe (KMI2019)* (2019), p. 19.

[32] Seiji Kawamura et al. “The Japanese space gravitational wave antenna: DECIGO”. In: *Classical and Quantum Gravity* 28.9 (2011), p. 094011.

[33] Maxim Yu Khlopov. “BSM Cosmology from BSM Physics”. In: *arXiv preprint arXiv:2112.03375* (2021).

[34] Edward Kolb. *The early universe*. CRC press, 2018.

[35] Mikko Laine and K Rummukainen. “What’s new with the electroweak phase transition?” In: *Nuclear Physics B-Proceedings Supplements* 73.1-3 (1999), pp. 180–185.

[36] Azadeh Maleknejad. “MPA Lectures on Gravitational Waves in Cosmology”. In: *Gravitational waves* 5 (), p. 2.

[37] Anupam Mazumdar and Graham White. “Review of cosmic phase transitions: their significance and experimental signatures”. In: *Reports on Progress in Physics* 82.7 (2019), p. 076901.

[38] Gaurav Narain, Jürgen Schaffner-Bielich, and Igor N Mishustin. “Compact stars made of fermionic dark matter”. In: *Physical Review D* 74.6 (2006), p. 063003.

[39] Avik Paul, Upala Mukhopadhyay, and Debasish Majumdar. “Gravitational wave signatures from domain wall and strong first-order phase transitions in a two complex scalar extension of the Standard Model”. In: *Journal of High Energy Physics* 2021.5 (2021), pp. 1–28.

[40] Mariano Quiros. “Finite temperature field theory and phase transitions”. In: *Proceedings, Summer school in high-energy physics and cosmology: Trieste, Italy* 1999 (1998), pp. 187–259.

[41] Denys Savchenko and Anton Rudakovskyi. “New mass bound on fermionic dark matter from a combined analysis of classical dSphs”. In: *Monthly Notices of the Royal Astronomical Society* 487.4 (2019), pp. 5711–5720.

[42] Suzanne Van Dam. “Spontaneous symmetry breaking in the Higgs mechanism”. In: (2011).

[43] Carroll L Wainwright. “CosmoTransitions: computing cosmological phase transition temperatures and bubble profiles with multiple fields”. In: *Computer Physics Communications* 183.9 (2012), pp. 2006–2013.

[44] David J Weir. “Gravitational waves from a first-order electroweak phase transition: a brief review”. In: *Philosophical Transactions of the Royal Society A: Mathematical, Physical and Engineering Sciences* 376.2114 (2018), p. 20170126.

[45] Xianhao Xin. *Glashow-weinberg-salam model: An example of electroweak symmetry breaking*. 2007.